ABSTRACT

Title of Thesis:	DESIGN AND ANALYSIS OF A NOVEL, ULTRA-LIGHT, CRYOGENIC DEWAR FOR BALLOON-BORNE OBSERVATORIES
	Samuel Adam Denker, Master of Science, 2020
Thesis Directed By:	Dr. Marino diMarzo Department Mechanical Engineering Department of Fire Protection Engineering

The deployment of cryogenic Dewars aboard high-altitude balloons is critical to astronomical observation at submillimeter wavelengths. Balloon-borne, cryogenically cooled telescopes are limited in size by weight restrictions of the balloons, which is dominated by the Dewars. This thesis presents a portion of the multi-phase BOBCAT project which reduces Dewar weight with the use of thin-walled designs and a novel multi-layer insulation (MLI) system. The BOBCAT-1 mission used conventional Dewar technology to demonstrate cryogen transfer at float altitude and establish baseline thermal performance of balloon-borne Dewars. Design and assembly of the BOBCAT-2 ultra-light Dewar showed successful fabrication of the thin-walled vessel and novel MLI system. Thermal modelling predicts that the BOBCAT-2 Dewar will experience an order of magnitude increase in heat transfer through the MLI, equivalent to a 60% increase through the Dewar in total, due to its larger volume and decreased number of radiation shields relative to the BOBCAT-1 Dewar.

DESIGN AND ANALYSIS OF A NOVEL, ULTRA-LIGHT, CRYOGENIC DEWAR FOR BALLOON-BORNE OBSERVATORIES

by

Samuel Adam Denker

Thesis submitted to the Faculty of the Graduate School of the
University of Maryland, College Park, in partial fulfillment
of the requirements for the degree of
Master of Science
2020

Advisory Committee:
Professor Marino diMarzo, Chair
Professor Jungho Kim
Research Professor Yunho Hwang
Dr. Alan Kogut

Dedication

To Amy, Mom, Dad, and Calvin.

Acknowledgements

First, thank you to Dr. Alan Kogut, my manager and PI at NASA Goddard, for giving me the opportunity to work under him on the BOBCAT project.

I would also like to send a special thank you to my adviser Dr. Marino diMarzo for making it possible to complete my thesis on this research while guiding me through the process.

Lastly, I would like to acknowledge the contributions of my coworkers to the work contained within this thesis and to making each day enjoyable. Paul Mirel, Nick Bellis, Mackenzie Carlson, and Danielle Sponseller, thank you.

The BOBCAT project is funded by NASA's Goddard Space Flight Center through the IRAD technology development program. My involvement in the project was supported by the Center for Research and Exploration in Space Science and Technology II (CRESSTII) cooperative agreement, number 80GSFC17M0002, task 665.006.

Table of Contents

List of Tables

List of Figures

List of Abbreviations

ARCADE - Absolute Radiometer for Cosmology, Astrophysics, and Diffuse Emission

BLAST - The Balloon-Borne Large Aperture Submillimeter Telescope

BOBCAT – Balloon-Borne Cryogenic Telescope Testbed

CSBF – Columbia Scientific Balloon Facility

MLI – Multi-layer insulation

NASA GSFC – National Air and Space Administration Goddard Spaceflight Center

PIPER – Primordial Inflation Polarization Explorer

RuOx – Ruthenium Oxide Resistive Temperature Detector

SMA – Submillimeter Array

SOFIA – Stratospheric Observatory for Infrared Astronomy

Chapter 1 Introduction

The deployment of telescopes aboard high-altitude balloons has long been a cost-effective way to perform ground-breaking astronomy. High-altitude balloons can rival satellites in signal quality over certain wavelengths when combining the advantages of altitude, cooled optics, and large collection area telescopes. Balloon-borne observatories routinely pass 30 km in altitude, above 99% of the mass of the atmosphere, greatly reducing photon emission and noise from the atmosphere. Cryogenically cooling the optical components below 10 K negates most of the emission and noise from the components of the telescope and payload. After this reduction in ambient brightness and noise has been achieved, increased collection area of the telescope allows for an increase in the signal of interest, both in magnitude and relative to noise. These advantages make distant and faint astronomical objects observable, including in the understudied submillimeter wavelength regime.

Aboard high-altitude balloons, weight restrictions impose harsh limits on telescope size, with the cryogen storage vessels, or Dewars, contributing the bulk of the parasitic mass. Therefore, engineering projects oriented towards reducing the mass of the Dewars can yield significant gains in telescope size and sensitivity. This thesis discusses a portion of the Balloon-Borne Cryogenic Telescope Testbed (BOBCAT) project, which is a multi-phase project with the goal of greatly reducing the weight of cryogenic Dewars for balloon-borne observatories. This thesis will cover aspects of two separate payloads. It will discuss the flight and data analysis of a conventional Dewar payload, BOBCAT-1, and the prototyping, assembly, and relevant preflight

analyses of the thermal and fluid performance of the ultra-light Dewar payload, BOBCAT-2.

Section 1.1: The BOBCAT Concept

The BOBCAT project from NASA Goddard Spaceflight Center (GSFC) is a multi-phase technology demonstration mission with the long-term goal of creating an ultra-light, cryogenic balloon payload for submillimeter astronomical observations. Through the BOBCAT-1 and BOBCAT-2 flight experiments, and potential future iterations, NASA aims to prototype and demonstrate an ultra-light weight Dewar concept, increasing the technological readiness level and bringing a 3-4-meter diameter submillimeter wavelength observatory at high altitude closer to reality.

This novel Dewar concept significantly reduces the weight of the conventional bucket Dewar with thin-walled construction. A bucket Dewar is designed for observations and has an open aperture on top with multi-layer insulation (MLI) between the bucket and the outer walls on the sides and bottom of the vessel. The MLI is kept in a vacuum that helps to reduce the heat transfer into the bucket. For the conventional bucket Dewar, this vacuum space is mechanically sealed and must withstand the 101 kPa pressure gradient present at sea-level. The ultra-light Dewar vacuum space is open on the ground and on ascent, where it continuously vents until float altitude, 24-40 km, is reached. The 24 km minimum float altitude has been established to ensure the payload ascends beyond the bulk of the mass of the atmosphere, while 40 km is a reasonable upper limit for scientific ballooning flights. At float altitude the vacuum space is sealed, and the remaining air is removed by freezing it onto the inner wall of the vacuum space when the bucket is filled with

cryogen. The maximum pressure gradient acting on the walls of the ultra-light Dewar is therefore only 3.0 kPa at 24 km in altitude. To allow for the air to vent as the payload ascends, the MLI within the vacuum space was changed from the conventional system of tightly packed reflectors and spacers to one of suspended concentric reflectors without a spacing material. The ultra-light Dewar concept is shown in Figure 1-1 and Figure 1-2 [1].

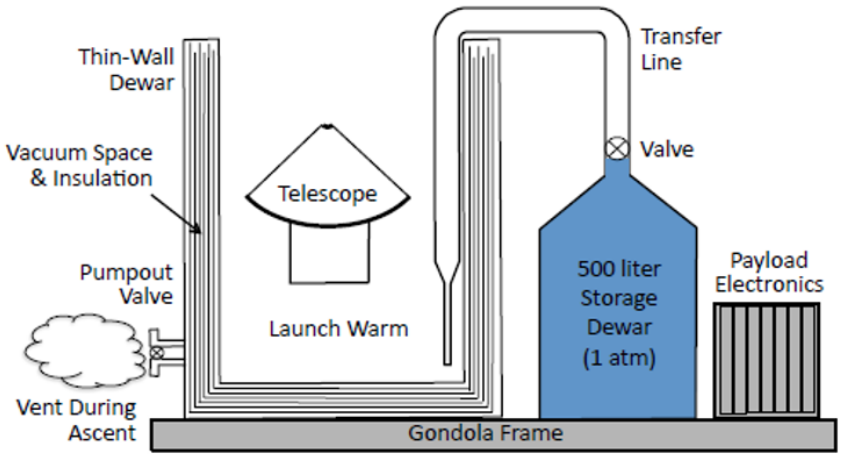

Figure 1-1: The BOBCAT concept; the BOBCAT ultra-light Dewar is launched warm and vents on ascent [1]

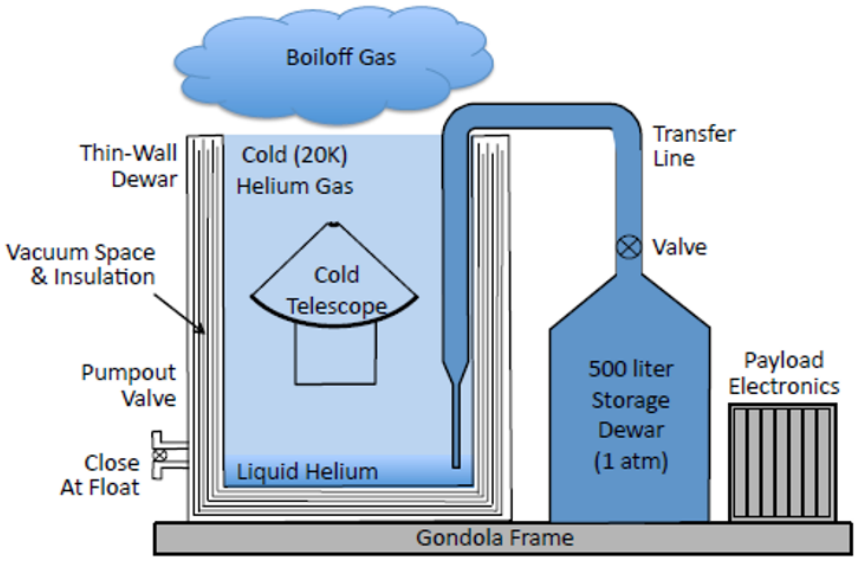

Figure 1-2: The BOBCAT concept; the BOBCAT ultra-light Dewar insulation is sealed and the bucket is filled with cryogen at float altitude [1]

The thin-walled construction is made possible by separating the task of cryogen storage from the bucket Dewar that is used to hold and cool the telescope in optic-carrying missions. The BOBCAT mission concept involves flying storage Dewars in addition to the bucket Dewar. These storage Dewars do not include the open aperture, are highly mass efficient, and have low cryogen boiloff rates. They therefore contribute minimal parasitic mass to the system. While the ultra-light Dewar is open on the ground and ascent, it does not function as an insulating vessel. Therefore, the cryogen is transferred from the storage Dewars to the bucket Dewar only once the bucket Dewar insulation space has been sealed at float altitude.

Section 1.2: The BOBCAT Flight Missions

The BOBCAT project will demonstrate task separation, cryogen transfer, and thin-walled construction with two flight missions. The BOBCAT-1 mission flew in August 2019, and the BOBCAT-2 mission is scheduled to fly in the fall 2020 launch

season. Both payloads carry liquid helium and liquid nitrogen storage Dewars for cryogen transfer at float altitude and electronics for controls, communication, and data logging. The difference between the two payloads is the bucket Dewar, which for BOBCAT-1 is a conventional bucket Dewar and for BOBCAT-2 is the first flight version of the ultra-light Dewar. Each Dewar has a 0.25-meter diameter bucket containing thermal and fluid instrumentation, and the dimensions, instrumentation, and cryogen transfer assemblies were kept as similar as possible between the two missions. This will allow for reasonable comparison of the thermal performance of each Dewar. As a technology demonstration mission, no telescopes will be flown aboard the BOBCAT payloads.

The two payloads also serve the following roles for validating the concepts of the BOBCAT project. BOBCAT-1 proved the process of transferring cryogen at float altitude, a first for a ballooning mission. Furthermore, the BOBCAT-1 flight provided the baseline data from a conventional Dewar necessary to show whether the ultra-light Dewar performs the task of cryogen storage and thermal management to a comparable degree. BOBCAT-2 will attempt to prove the concept of venting the vacuum space on ascent and sealing the vessel at float. It will also demonstrate the effectiveness of cryoplating. For the ultra-light Dewar, cryoplating is the means of creating a vacuum jacket around the bucket, and it is advantageous because it requires no additional components beyond the valve that seals the vacuum space. As the Dewar is filled with cryogen, the bucket will cool rapidly, and the remaining air in the vacuum space will freeze onto the shared wall with the bucket. Once achieved, the interstitial pressure in the vacuum space will be significantly reduced, and the heat transfer via convection

will become negligible. As BOBCAT-2 repeats the flight parameters from BOBCAT-1, it will show that the heat flux into the Dewar can be adequately controlled by the new system of concentric radiation shields necessitated by the thin-walled design. To this end, thermal models developed prior to the flight of BOBCAT-2 will be important for determining expected results and comparing to the flight results of both the BOBCAT-1 and BOBCAT-2 flights. Accurate modeling will inform on feasibility and scalability of the ultra-light Dewar concept in advance of potential future iterations.

Section 1.3: Thesis Roadmap

An overview of the novel contributions and relevant prior work of this thesis is discussed in this section. Work on both BOBCAT payloads began prior to the starting point of this thesis. This prior work will be discussed in detail in Section 3.1 for BOBCAT-1 and Section 4.1 for BOBCAT-2. Additionally, Chapter 2 will present a literature review of the underlying physics and technologies of balloon-borne, cryogenic payloads.

The new work on BOBCAT-1 begins with its launch from Ft. Sumner, New Mexico in August 2019. The launch involved ground and compatibility testing, launch operations, and conducting the flight experiments of cryogen transfer and helium boiloff observations at float altitude. Following the flight, data analysis was conducted to establish the baseline performance for comparison to the BOBCAT-2 flight.

For BOBCAT-2, the new work began by taking the initial design of the BOBCAT-2 payload to assembly of the flight vessel. This involved assembling laboratory prototypes of the ultra-light Dewar to improve the design and assembly process of the flight vessel. Concurrently, multiple models were developed of the

thermal and fluid processes important to success of the mission. These included calculations to predict the behavior of air in the vacuum space during ascent of the payload, predictions of the volume of cryogen needed for the experiment, and detailed thermal models of heat transfer through the MLI.

The contributions of this thesis have been organized into three main chapters. Flight and analysis of BOBCAT-1 will be detailed in Chapter 3. Prototyping and assembly for the BOBCAT-2 ultra-light Dewar will be detailed in Chapter 4. The thermal and fluid investigation of the expected performance of the ultra-light Dewar is then covered in Chapter 5. Lastly, Chapter 6 will conclude on the work that has been presented here and discuss future work for the BOBCAT project.

Chapter 2 Literature Review

The work contained within this thesis is predicated on three interconnected topics. This chapter will provide a review of prior research on astronomy aboard airborne platforms, Dewars and MLI, and the heat transfer environment of a high-altitude balloon, including external, atmospheric effects, and the behavior of cryogens in the Dewar.

Section 2.1: Airborne Astronomy

Submillimeter astronomy involves observing a range of electromagnetic radiation wavelengths between infrared and radio waves, generally considered to be 0.3-1.0mm. These wavelengths play a unique role in modern astronomy yet are understudied. For example, observations of the submillimeter regime have been used to better understand star forming regions of the early universe [2,3]. Future investments in the study of the submillimeter wavelength range appear forthcoming, and because the transmissivity of the atmosphere to these wavelengths is low, many of these observatories will be space-based, such as the Origins Space Telescope [4]. The main drawback to space-based observatories is cost and development time. Therefore, improvement in ground or airborne observatories in the submillimeter regime could offer advantages that lead to a significant increase in the quality and quantity of observations in the submillimeter regime.

Ground and airborne observatories targeting the submillimeter regime must contest with the challenges presented by observing through the atmosphere. The Submillimeter Array (SMA) is a state-of-the-art ground-based observatory that sits on Mauna Kea, Hawaii at 4 km of elevation [5]. This elevation is important for reducing

emission and noise from the atmosphere, increasing the sensitivity of the SMA compared to sea-level observations. For airborne observatories, the Stratospheric Observatory for Infrared Astronomy (SOFIA) flies at an altitude of 14 km [6]. Balloon-borne observatories can reach altitudes of up to 40 km. Figure 2-1 presents the atmospheric emission present at altitudes of 14 km and 40 km in red and blue lines, respectively [1]. Beyond the use of altitude to increase the transmissivity of the atmosphere to submillimeter wavelengths, cryogenically cooled optics are also greatly beneficial. As Figure 2-1 shows, the emission from uncooled optics drowns out the signals of interest. With the combination of cryogenic cooling and deployment of observatories at 40 km in altitude, the final step required to approach the sensitivity of space-based missions from balloon-borne observatories is to increase signal level by increasing the collection area of the telescope. As a benchmark, a state-of-the-art space-based observatory, the Herschel Space Observatory, flew a 3.5-meter diameter primary mirror cooled to 70 K [7].

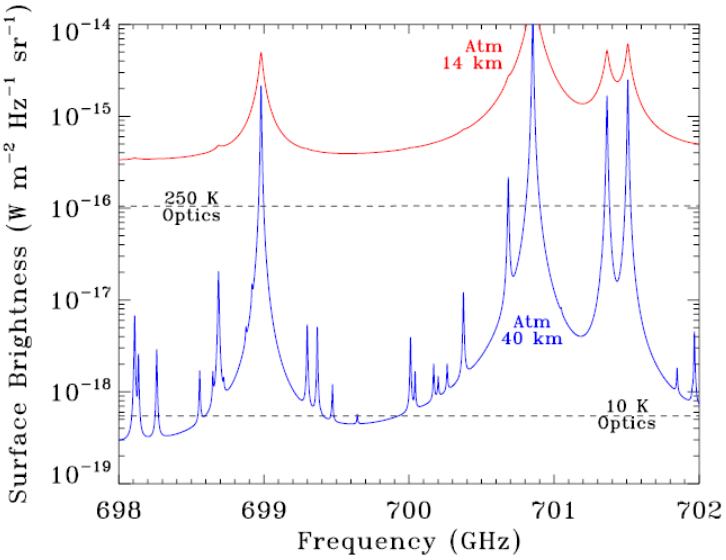

Figure 2-1: Atmospheric and temperature effects on submillimeter observations from airborne observatories [1]

Examples of current state-of-the-art balloon-borne observatories include the prior flights of the PIPER [8], ARCADE-2 [9], and BLAST [10] missions. Both the Primordial Inflation Polarization Explorer (PIPER) and the Absolute Radiometer for Cosmology, Astrophysics, and Diffuse Emission (ARCADE-2) payloads approached the weight limits for balloon-borne missions and contained 1-meter diameter optics cooled to 1.5 K that necessitated 800 kg cryogenic Dewars for cooling. If the optics were scaled to the 3-meter diameter optics achievable by space missions, the estimated Dewar mass of 5000 kg would surpass the 2800 kg lift capacity of standard balloons [1]. The Balloon-Borne Large Aperture Submillimeter Telescope (BLAST) flew a 2-meter diameter telescope at intermediate temperatures (between cryogenic and ambient) adapted from the Herschel telescope [10]. The PIPER, ARCADE-2, and BLAST missions show the nature of the relationship between the degree of cooling, the weight of the Dewar, and the size of the telescope flown.

Section 2.2: Dewars and Multi-Layer Insulation

Cooling and housing balloon-borne telescopes is often accomplished with vacuum-jacketed vessels for cryogen storage, or Dewars. Dewars serve to insulate cryogenic liquids from the external environment and maintain their low temperatures. The operating principle of a Dewar is the creation of an insulated vacuum jacket surrounding the cryogen. The vacuum removes convection as a heat transfer mode into the cryogen, and the insulation minimizes the conduction and radiation. As the literature shows, numerous highly specialized Dewars have been developed from these simple operating principles. Urban performed numerous analyses of spacecraft Dewars including the Dewar for the space-based Infrared Telescope [11]. This Dewar was a state-of-the-art storage Dewar for spaceflight and contained 250 L of liquid helium at 1.6 K. The Dewar system included transfer assemblies, instrumentation, and MLI around the storage vessel. Additionally, Fleener worked to develop a low-cost, long-life Dewar for the Space Infrared Telescope Facility [12]. The long lifetime of cryogenic fluids in a conventional, thick-walled Dewars is the main advantage of these Dewars and the reason they are used for spaceflight missions. Lastly, Pereguda discussed the manufacturing of thin-walled Dewars for agricultural applications by welding specialized alloys [13]. While not built for space or high altitude, the manufacturer utilized welding of thin materials akin to the manufacturing of the BOBCAT ultra-light Dewar.

To allow the telescope aboard high-altitude balloons optical access to the observational target, a bucket Dewar is often used. Bucket Dewars are less efficient than conventional Dewars, as they afford a direct path for heat transfer to reach the

optical components. This path includes conduction down the walls of the bucket and heat transfer directly through the gas, either by convection or radiation from the atmosphere. The cryogen in the bucket serves to counter the excess heat and keep the components cool as the boiloff of the cryogen in the bucket removes the excess heat. The vacuum insulation of the bucket Dewar is then used to minimize the heat transfer from the sides and bottom of the Dewar relative to the heat transfer through the open aperture. For comparison, where cryogen can survive in a conventional Dewar for spaceflight for a year or more, bucket Dewars for ballooning missions are designed for cryogen lifetimes on the order of a day. Figure 1-2 presented a schematic of a bucket Dewar, the BOBCAT ultra-light Dewar concept, while Figure 2-2, courtesy of PIPER principal investigator Dr. Alan Kogut, presents an up-to-date schematic of the PIPER bucket Dewar, including its open aperture and telescope assemblies.

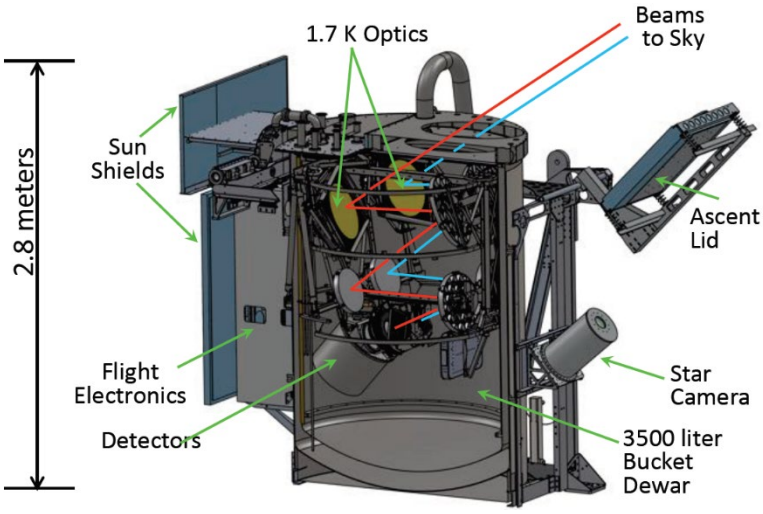

Figure 2-2: The PIPER telescope contained within a bucket Dewar (courtesy of Dr. Alan Kogut)

Many advances in Dewar technology are dependent on advances in MLI. MLI refers to the use of multiple layers of reflective material, or radiation shields, tightly spaced with low conductivity materials to greatly reduce heat transfer through a vessel.

In Dewars, the MLI is found in the vacuum space, so that convection is negligible, and conduction and radiation are minimized. Due to its importance for spaceflight and other industries, numerous advances in the study of MLI have been made in recent decades. Fesmire and Johnson compiled an extensive list of MLI studies that provide a meaningful baseline for the effectiveness of different reflector/spacer combinations, number of layers per centimeter, and total number of layers [14]. These combinations include reflective materials such as double-sided aluminized Mylar or aluminum foil, and spacer materials such as paper or silk netting. Augustynowicz and Fesmire discussed a novel MLI system for an imperfect vacuum with interstitial pressures on the order of hundreds of Pascals. This level of interstitial pressure requires a novel insulation system due to the degradation of MLI efficiency once interstitial pressure surpasses 10^{-1} Pa [15]. For spaceflight, MLI systems are often launched in ambient pressure before using the vacuum of space to vent the insulation. Riesco et al. showed that vented MLI systems could take 50 hours to vent and achieve optimal thermal performance and discussed how perforations to the MLI have been used to increase the vent rate [16]. Johnson discussed the mass and insulation efficiency of MLI for varying numbers of layers per thickness of the MLI and found that systems with 2 layers per millimeter were optimal [17]. Lastly, multiple studies have discussed the transmissivity of the reflective layers to wavelengths of thermal emission associated with low temperature materials and found that transmissivity is negligible in MLI systems [18,19].

Section 2.3: High-Altitude Balloon Thermal Environment

The last topic to be reviewed in this chapter is the thermal environment experienced by a high-altitude balloon payload at float altitude. This includes both external, atmospheric effects, as well as heat flow within the Dewar and stored cryogens. This section will discuss heat transfer in the atmosphere and the behavior of liquid helium at float altitude.

The atmospheric thermal balance is shown in Figure 2-3 [20]. Considering Figure 2-3, for the payload of the balloon, the inner skin terms and internal reflections can be disregarded. The thermal balance during the day includes direct solar radiation, typically denoted as G, infrared radiation from the earth, and infrared radiation from the gas and clouds in the atmosphere. Solar radiation also reaches the payload by albedo reflection from the earth and clouds, or $\rho*G$, where ρ is the albedo factor, which ranges from 0-1. Heat leaves the payload by radiation outward and convection to the atmosphere, both captured in the outer skin heat flux term from Figure 2-3.

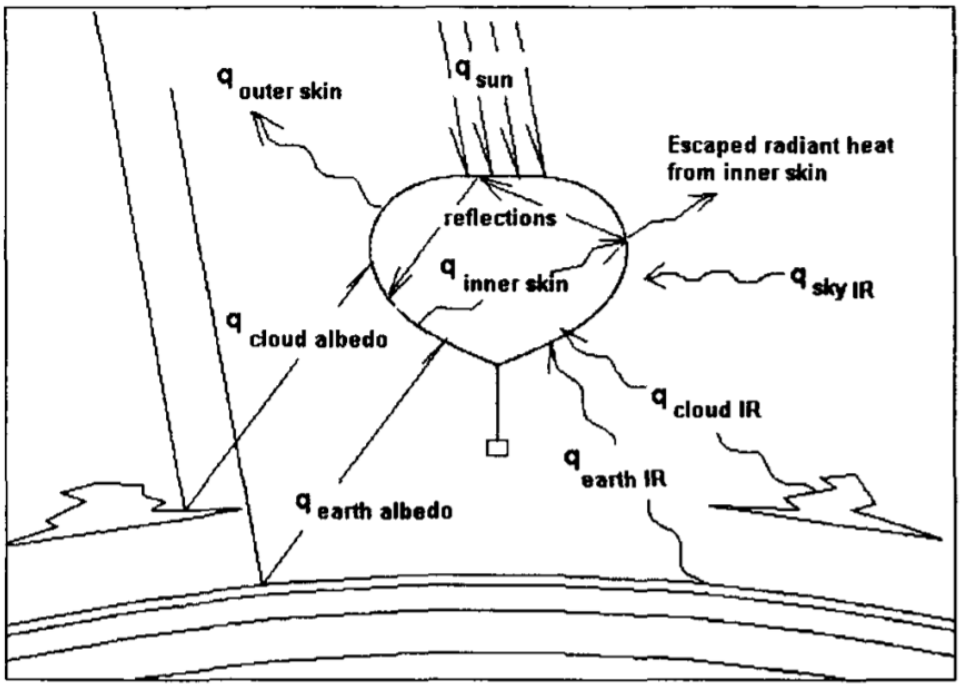

Figure 2-3: Thermal balance of high-altitude balloons [20]

Kreith and Warren presented the relative magnitudes of the different heat transfer modes at 21 km in altitude [21]. At this in altitude, direct solar radiation is typically 1390 Wm^{-2}, in the middle of the day, and acts over the projected area of the payload relative to the solar angle. Reflected solar radiation, or albedo radiation, acts in a diffuse manner over the bottom of the payload, contributing as much as 360 $Wm-^{2}$. Infrared radiation from the earth and the atmosphere combined were 130 Wm^{-2}. Heat out of the payload was then determined from a combination of emitted radiation and convection, where emission is typically dominant, and convection decreases for higher altitudes. Lastly, Kreith and Warren reported that the balloon payload experienced an average atmospheric temperature of 237 K at 21 km, where the payload warmed to as much as 278 K. For higher flights, they anticipated an atmospheric environment of 250 K at 40 km, where the payload would warm to 266 K [21]. This data will be critical for determining the boundary conditions of the thermal analyses in Chapter 5.

For the bucket Dewars that house the optics on high-altitude balloon flights, the heat that reaches the inside of the bucket is removed by boiling the helium within the bucket. Helium is used aboard cryogenic balloon payloads because it is highly transmissive to the signals of interest and pools below 2 K at a saturated vapor pressure of 10^3 Pa. Figure 2-4, from the summary of superfluid helium research by Donnelly, shows that at the pressure of the atmosphere at 24 km and above, 2950 Pa and lower, the liquid helium will exist in the He-II, or superfluid, phase [22]. The boiling of superfluid helium is a different mechanism than that of a normal liquid; superfluid helium presents the qualities of superconductivity, which greatly changes the nature of boiling [23]. Filina discusses this boiling process and reports that due to the superconductivity, heat flux from a warm surface is transported to the phase interface, where evaporation of the superfluid occurs [23]. Throughout this thesis, the phase change of the superfluid helium within the bucket will be referred to as the boiloff process. The ARCADE-2 project demonstrated an important aspect of bucket Dewars containing superfluid helium. As the superfluid helium boiled off in the bucket, it created a barrier of helium gas in the aperture the prevented the ingress of atmospheric gases to the Dewar [9].

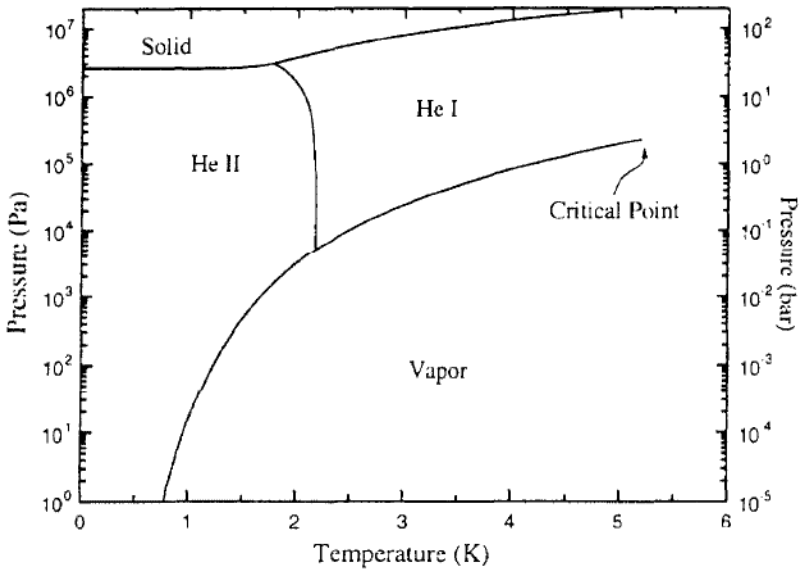

Figure 2-4: Phases of helium with temperature and pressure [22]

Chapter 3 BOBCAT-1

The BOBCAT-1 mission was flown to demonstrate cryogen transfer at float altitude and establish baseline data from a conventional bucket Dewar for comparison to the ultra-light Dewar. Development of the BOBCAT-1 mission began in October 2017, before the start of this thesis. The payload launched in fall 2019, and the launch and post-flight data analysis are included here. This chapter will begin with an overview of the prior work on the BOBCAT-1 mission, Section 3.1, proceed to the pre-flight operations, Section 3.2, the flight of the payload, Section 3.3, and close with the analysis of the flight experiments conduction, Section 3.4. This mission was covered in detail in Kogut and Denker et al. [1].

Section 3.1: BOBCAT-1 Prior Work

BOBCAT-1 was designed and assembled prior to the start of 2019. Figure 3-1 shows the design of the fully assembled BOBCAT-1 payload. Mounted on the gondola of the payload are liquid helium and liquid nitrogen storage Dewars, telemetry and electronics boxes, and the conventional bucket Dewar. The liquid helium and liquid nitrogen Dewars store 500 and 80 liters (L), respectively. Each storage Dewar is outfitted with the necessary transfer components, such motorized valves to control the flow to the receiving bucket Dewar. Internally, the storage Dewars contain boiloff heaters to remove excess cryogen after the flight experiment is complete. The telemetry serves to report the position, heading, and altitude of the balloon. The position and heading are controlled by the wind, but ballast can be dropped to achieve higher altitude and ascent rate. The telemetry box also included a downlink to allow for

communication with the onboard computers. The electronics box contains the relevant payload electronics, such as the flight computer and readouts for the instrumentation within the various Dewars and transfer assemblies. Additionally, attached to the gondola is a video camera pointed at the vent of the conventional bucket Dewar. The camera was intended to monitor the outside of the vent for visible ice buildup, potentially indicating atmospheric gases entering the bucket of the Dewar, which would affect the observation quality of telescope carrying missions.

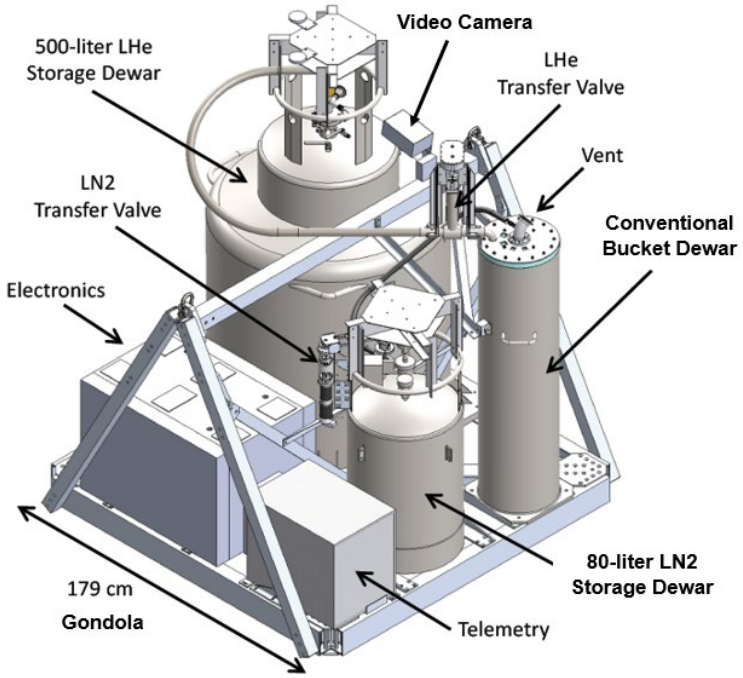

Figure 3-1: The BOBCAT-1 payload design

The last component of the BOBCAT-1 payload is the conventional bucket Dewar. This Dewar has a 25 cm diameter bucket, 122cm deep, with 5 cm of radial space for MLI. It can hold up to 60 liters of cryogen. The bucket Dewar includes a 5 cm vent, which acts as the open aperture of the bucket, contributing additional thermal load while allowing the boiloff gas to vent. The remainder of the bucket is covered by a lid which suspends an insert into to the bucket Dewar, shown schematically in Figure

3-2. The insert contains the outlets for the liquid nitrogen and liquid helium transfer lines, multiple pairs of temperature sensors, both discrete and continuous level sensors, and two boiloff heaters. The pairs of temperature sensors consist of Lakeshore DT-670 silicon diodes and Ruthenium Oxide resistive temperature detectors, or RuOx sensors, where the diodes cover the temperatures from 300-30 K, and the RuOx sensors cover below 30 K. The level sensors, discrete and continuous, are also paired to ensure accurate readings. Six discrete level sensors are positioned intermittently up the height of the bucket and offer a binary reading of whether the level of superfluid helium is above or below each sensor. These discrete level sensors consist of a small resistive heater and a RuOx sensor. When the heater is powered, the reading of the RuOx sensor increases by several Kelvin if the sensor is not submerged in superfluid helium and does not increase if it is submerged. The continuous level sensors were superconducting level sensors purchased from American Magnetics. The operation of the continuous level sensors differs, as they return the exact height of superfluid helium in the bucket from the voltage drop along the sensor. Detailed operation of the continuous level sensors will be discussed in Section 3.3. Lastly, the boiloff heaters for the conventional Dewar serve the same role as those in the storage Dewars – to boiloff excess cryogen after the experiment so the Dewar contains no cryogen on descent and landing.

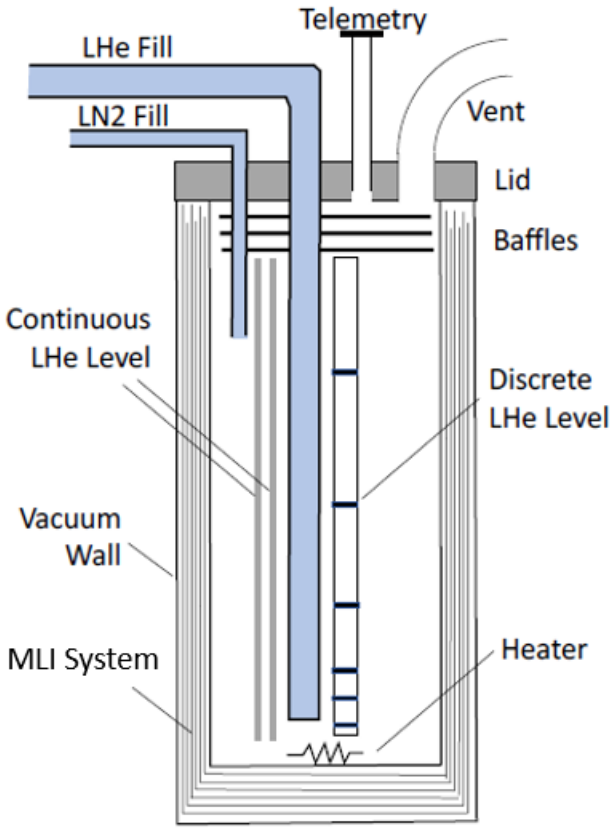

Figure 3-2: Dewar insert schematic with instrumentation and transfer assemblies [1]

Many of the BOBCAT-1 flight components previously described are necessary for the transfer of cryogens between the storage Dewars and the bucket Dewar. The pressure maintained within the storage Dewars is much higher than the ambient pressure at the minimum float altitude of 24 km. Therefore, the transfer process is controllable by a single motorized valve for each storage Dewar. For the liquid nitrogen transfer, the receiving environment of the bucket Dewar near 1 kPa is much lower than the 12.5 kPa triple point of liquid nitrogen [24]. For the nitrogen transfer, it is expected that the nitrogen will freeze into a "snow" in the bucket before sublimating. This phenomena of the nitrogen ice buildup in a bucket Dewar was experienced by the ARCADE-2 mission [9]. As shown by the helium phase diagram from Section 2.3, the

liquid helium is expected to transition to superfluid during the transfer, which would induce boiloff that could contribute back pressure to the transfer line and reduce or stop the transfer process. Demonstrating that these phase transition processes do not prevent cryogen transfer was a major goal of the BOBCAT-1 flight. Section 3.4 will show that this goal was achieved.

In addition to the design and assembly of the BOBCAT-1 payload, the flight plan for the mission was developed. The flight plan included launching the payload with the bucket Dewar empty and performing a pre-cool operation before filling the bucket Dewar. The pre-cool uses liquid nitrogen, with nine times more latent heat of vaporization than liquid helium, to cool the vessel to around 100 K. Once the nitrogen sublimates away, liquid helium is transferred to further cool the vessel, where it transitions to superfluid and then fills the bucket. The experiment to determine the baseline performance data is then conducted. This experiment involves filling the bucket to a known volume of superfluid helium and allowing it to boil off. Over the course the boiloff experiment, the level of superfluid helium is carefully monitored to determine the heat transfer into the bucket calorimetrically from the boiloff.

Section 3.2: Pre-Flight Operations

The novel work of this thesis on the BOBCAT-1 mission begins with the preparations for launch of the payload from Fort Sumner, New Mexico. The most important aspect of the pre-flight operations was the compatibility test run by Columbia Scientific Balloon Facility (CSBF), who provide the launch, and the BOBCAT team. The compatibility test of the BOBCAT-1 payload included a pre-flight weight measurement, where the payload weighed in at 850 kg. The compatibility test also

included communicating with the payload through the CSBF remote telemetry. Both the CSBF and BOBCAT teams communicated with and controlled the payload during the flight; CSBF monitored payload position, altitude, heading, and weather conditions, while the BOBCAT team controlled the experiment operations. For the compatibility test, each team ran through their expected flight procedures while the other team monitored the telemetry for interference between the two teams' procedures. The test was successful, verifying that communication with the payload would run smoothing.

Additional pre-flight tests including the dry run and cryogen transfer tests conducted by the BOBCAT team. For the dry run, the flight experiment was practiced without cryogens while improving the flight plan. Some of the practice commands included powering on and off each of the flight controllers, turning on the video camera, and cycling each motor. For the cryogen transfer test, both nitrogen and helium were transferred slowly until the temperature and level sensors within the bucket Dewar confirmed receipt of the cryogen. On the ground, this was also readily apparent from the large plumes exiting the vent of the bucket Dewar. Following these tests, the BOBCAT team declared the payload flight ready, which was followed by filling the storage tanks with the proper cryogenic liquids and waiting on the weather for acceptable flight days. The fully assembled and flight ready BOBCAT-1 payload is shown in Figure 3-3.

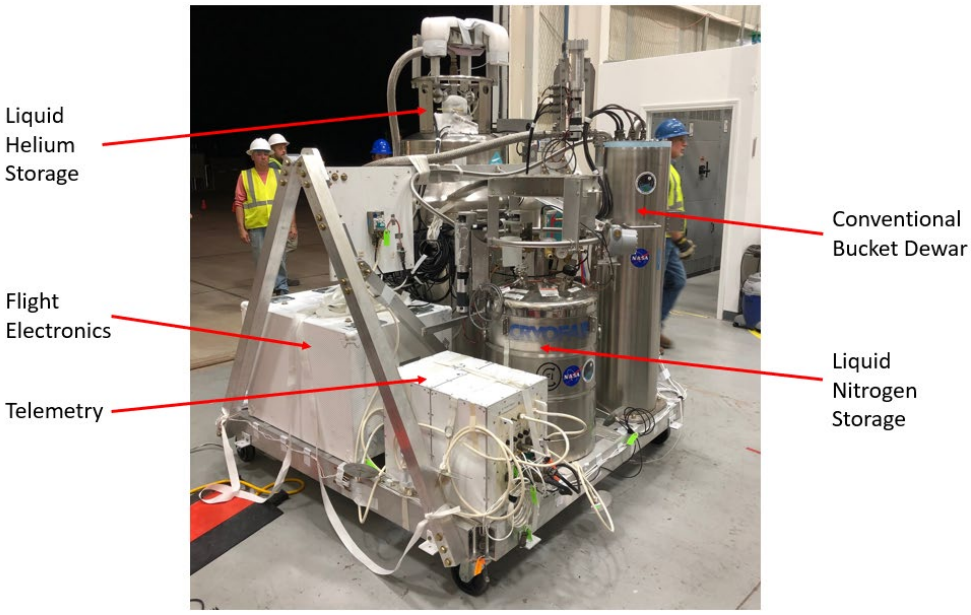

Figure 3-3: The BOBCAT-1 payload on the morning of launch

Section 3.3: The BOBCAT-1 Flight

The BOBCAT-1 payload launched at 7:59 am MDT, on August 22nd, 2019. The payload flew to 39.7 km aboard a 0.84 million cubic meter balloon, reaching float altitude by 10:52 am. Liquid nitrogen transfer began slightly before this, at 10:38 am, and was finished by 11:30 am. The liquid helium transfer began at 11:46 am, and by 12:09 pm, the bucket Dewar was filled roughly half full, containing 31 L of superfluid helium. The boiloff experiment was then conducted, which will be discussed, in detail, shortly. The experiment was completed by 1:54 pm, when preparations for cutdown from the balloon were made. The preparations involved boiling off all remaining liquid and superfluid helium with the heaters to ensure a safe landing and recovery. This boiloff lasted until 2:28 pm, and the payload was released from the balloon at 3:28 pm. The payload was subsequentially recovered undamaged by the CSBF recovery team.

All told, the payload was at a float altitude for five hours, of which four hours were used for the cryogen transfer and boiloff experiment.

The first task, once at float altitude, was to perform the cooling operations on the test Dewar. Liquid nitrogen was used to begin the cooling, due to its large latent heat of vaporization, nine times that of the helium. To avoid leaving nitrogen ice in the bucket Dewar once the helium was added, the nitrogen was only used to cool the Dewar from the 290 K starting temperature of the bucket at float altitude to 100 K. The nitrogen pre-cool operation took three fills of spraying the nitrogen into the bucket and allowing it to sublimate and cool the Dewar. The fill operations were done in spurts to avoid the potential for nitrogen ice to build below the transfer line motor such that it would be unable to close. On the third fill, the nitrogen motor did collect enough ice to not seal completely, and the solution was to turn the motor heater on for five minutes before proceeding. During this time, there was also a small amount of nitrogen ice in the bottom of the bucket Dewar, so the boiloff heater was turned on briefly to sublimate this buildup. After the nitrogen pre-cool, the Dewar was further cooled with liquid helium from 100 K down to the temperature of the saturated superfluid helium at 300Pa, 1.3 K. Once adequately cooled, the helium could pool in the bucket, and the bucket was filled to 31 L and monitored as it boiled off.

Section 3.4: BOBCAT-1 Results and Analysis

The BOBCAT-1 mission was successful in demonstrating cryogen transfer at float altitude and supplying baseline thermal data for future iterations of the project, notably BOBCAT-2. The first result of the BOBCAT-1 mission was that cryogen transfer was successful. From the cooling operations, this can be seen from the drop in

Dewar temperature associated with opening the transfer valves, shown in Figure 3-4, where diode reading refers to the DT-670 silicon diode and RuOx reading refers to the Ruthenium Oxide RTD.

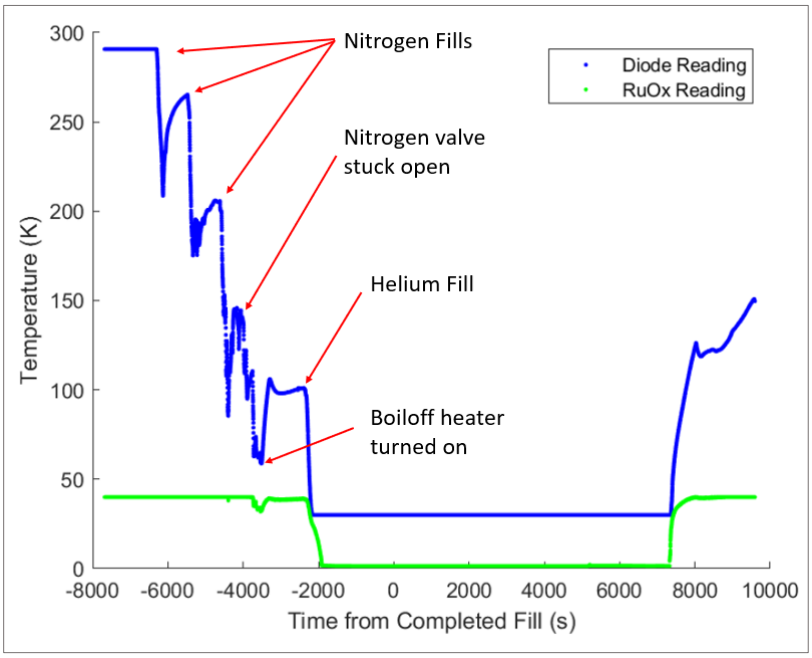

Figure 3-4: Temperature readings from the sensors at the bottom of the bucket Dewar

Successful cryogen transfer was also proven by the readings of the continuous level sensors from American Magnetics, which showed 31 L of superfluid helium filling the bucket (Figure 3-5). The continuous level sensor was the primary instrument for the flight experiment. It was used to record the level of superfluid helium in the bucket Dewar, which validated the cryogen transfer process and recorded the helium boiloff process. The continuous level sensor functions as a variable resistance wire extended the vertical length of the bucket. The wire is superconductive below 4.2 K and has a finite resistance above 4.2 K. The wire is fed a constant current, such that a measurement of the voltage drop is directly proportional to the percentage of the wire that is submerged in superfluid helium, where no voltage drop would represent fully

submerged. The exact equation for this translation is therefore shown by equation (3-1).

$$Level\ (liters) = \left(2 + 36 * (1 - \frac{V}{29.4})\right) * 1.29 \tag{3-1}$$

From equation (3-1), the 36-inch level sensors are 2 inches from the bottom of the Dewar, the supply voltage is 29.4 V, and the geometry of the bucket determined that each inch depth of superfluid helium translates to 1.29 liters. As a result of this operation, the wire dissipates energy by Joule heating, equation (3-2), where P is the dissipated power, I is the current and V is again the voltage.

$$P_{gen} = I * V \tag{3-2}$$

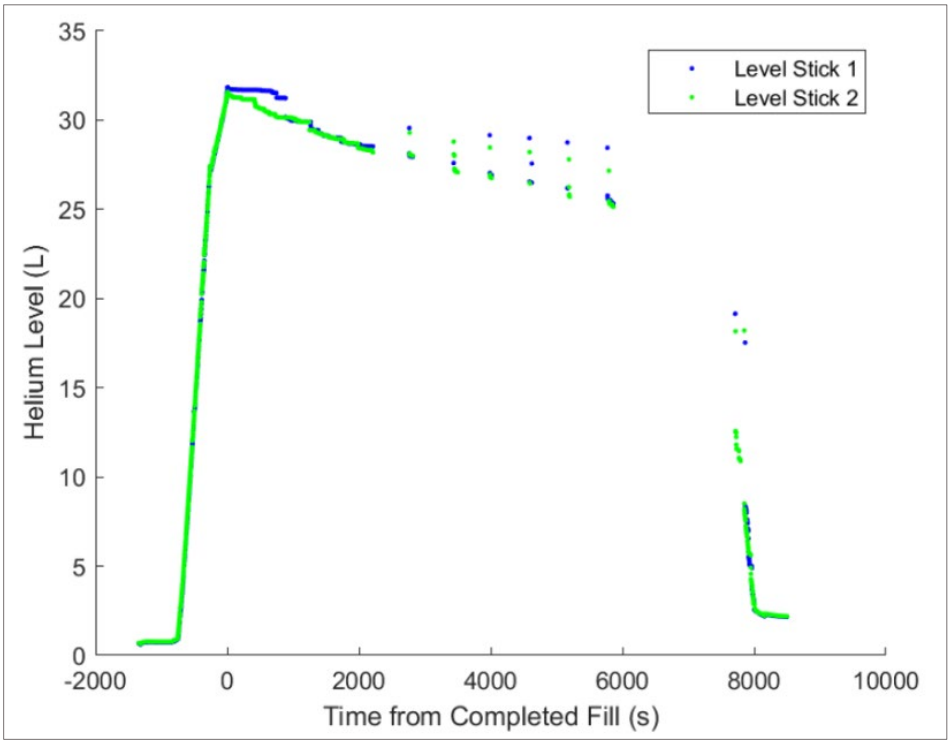

Figure 3-5: Volume of superfluid helium measured by the two level sticks

The calculated level of superfluid helium in the bucket over the duration of the experiment is shown in Figure 3-6. As planned, there were two sections to the

experiment, one where the level sticks were left on continuously to show the steady rate of boiloff, and the other, where the sensors were only turned on for brief enough time to stabilize to the correct level without generating excessive heat. This was done because the rate of heat generation from the level sensors was significant. The data from each portion of the experiment is treated separately, below.

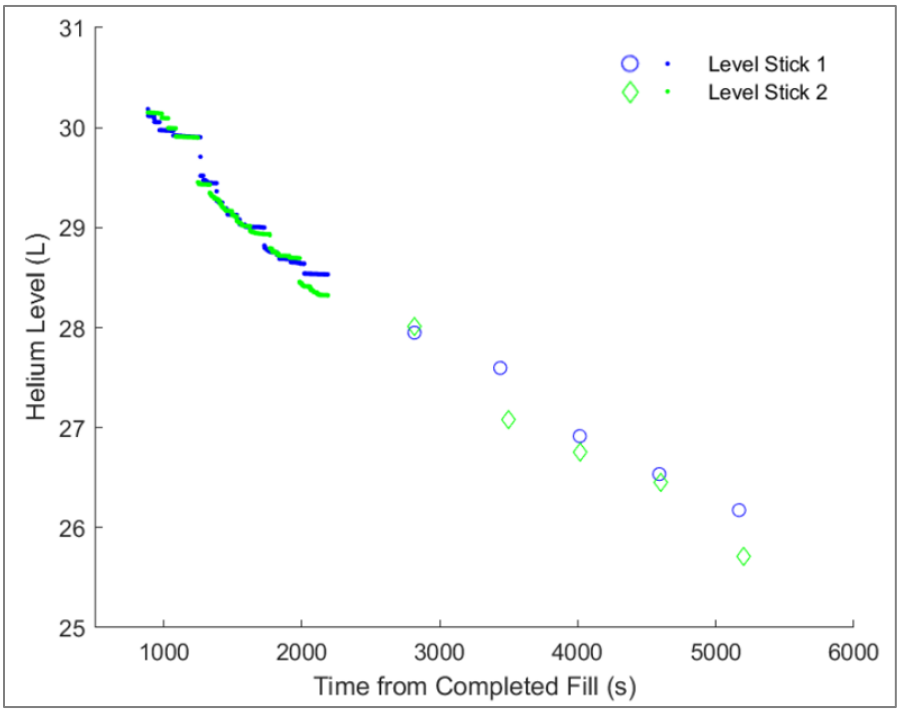

Figure 3-6: Level of helium in the bucket Dewar during the continuously and discretely measured portions of boiloff

For the portion of the experiment with the level sensors on continuously, the boiloff rate was determined to be 5.4±0.2 L/hr, and for the discretely measured portion, the boiloff rate was 3.2±0.3 L/hr. The boiloff rate of the superfluid helium was used as a calorimetric measure of the heat transfer to the superfluid helium. This calorimetric experiment simplifies the study of the heat transfer in the bucket Dewar by ignoring the complex nature of the boil and flow of the helium gas out of the bucket in favor of focusing only on the level of superfluid helium. The translation from boiloff to heat

transfer reaching the superfluid helium uses a density of 0.145 g/cm^3 and the latent heat of 86 J/mol to determine a conversion rate of 3062.5 J/L for 1.3 K superfluid helium at the saturated vapor pressure [22]. This results in total heat transfer values of 4.7±0.2 W and 2.8±0.2 W for the two parts of the experiment. These values were then corrected for the heat generation by the level sensors. Using the Joule heating as determined in equation (3-2), the level sensors dissipated 1.8 W when in continuous operation and generated 280 J, total, during the discrete measurement portion of the experiment. This results in corrected values of heat gain of 2.8±0.2 W and 2.7±0.2 W for the active and passive sections, which are in good agreement. These values will be used for a like for like comparison of the heat gain in the BOBCAT-2 ultra-light Dewar, which will employ the same experimental scheme.

After the determination of the total heat transfer to the superfluid helium, individual heat paths were considered. Derivation of the heat paths proved difficult with the deployed sensor scheme, which was optimized to determine the boiloff rate of the superfluid helium in the bucket. The heat paths that were considered are listed below and shown in Figure 3-7. This figure shows a cross section of the ultra-light Dewar, yet the heat transfer paths will remain the same for both the ultra-light and conventional Dewars.

1. Conduction down the walls of the bucket and the insert
2. Heat transfer through the MLI
3. Heat transfer through the lid of the Dewar
4. Heat generation by the sensors

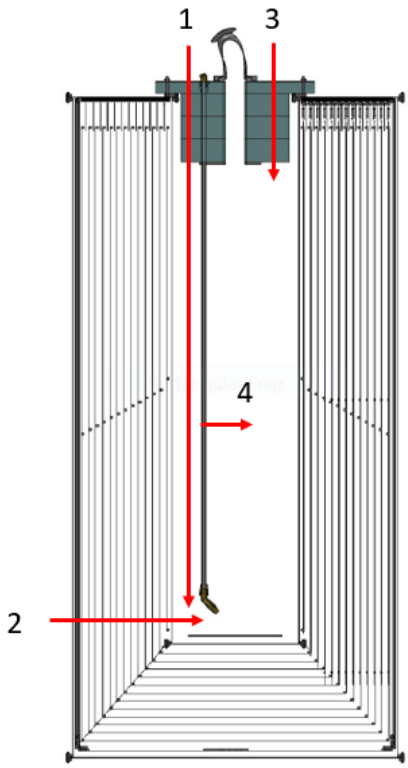

Figure 3-7: Heat transfer paths in the bucket Dewar

From the list above, heat transfer path 1 is counteracted by convection to the helium gas. Data from the BOBCAT-1 flight shows that this interaction is likely critical to understanding the exact nature of the heat transfer in the bucket. A temperature gradient built up in the helium gas in the bucket, due to the relatively low boiloff rate and stratification of the gas within the bucket. While the level of superfluid helium in the bucket dropped, the temperature recorded under the lid of bucket grew. At 31.5 L (62 cm) of superfluid helium in the bucket, the temperature difference between the lid and the fluid was 25 K. With 25.3 L (50 cm) of superfluid helium in the bucket, this difference was 65 K. The temperature below the lid of the bucket as the level of superfluid helium drops is shown in Figure 3-8. This temperature profile in the bucket demonstrates that the gas contributes to removing heat from the bucket Dewar, yet the

instrumentation flown for BOBCAT-1 was insufficient to determine the amount of heat removed by the flow of helium gas during the boiloff experiment.

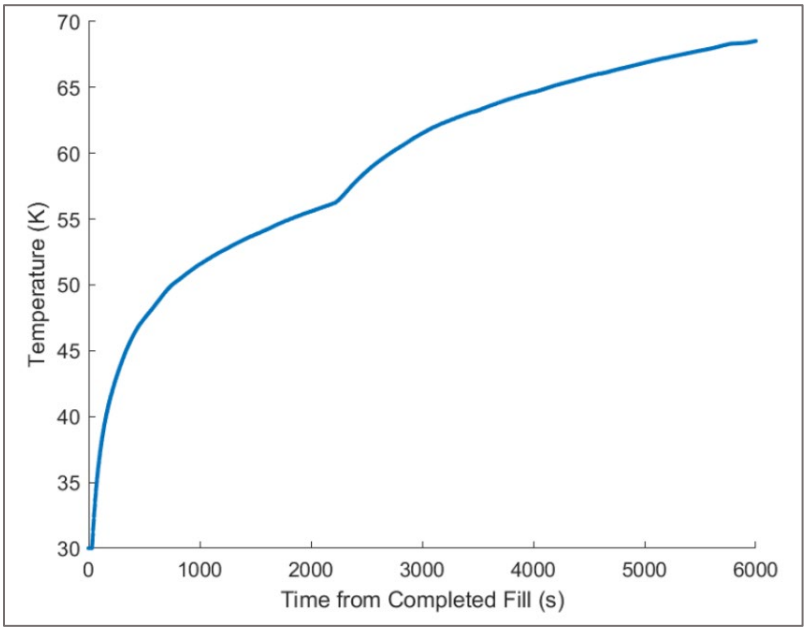

Figure 3-8: Temperature recorded below the lid of the bucket Dewar during the boiloff experiment

Of the remaining heat transfer paths, the heat through the lid and the generation by the remaining sensors were negligible. The conduction through the lid would only reach the gas that was flowing out of the bucket and could not contribute significantly to the helium boiloff rate. Based on the low temperatures recorded in Figure 3-8, radiation from the lid into the bucket is similarly negligible. The sensors that have not been considered to this point operated on 30 V flight batteries but drew currents on the order of milliamps, so Joule heating would be negligible.

The last heat transfer path to be considered, which is the most important for comparison to the ultra-light Dewar, was the heat flux through the insulation. While the construction of the conventional bucket Dewar for BOBCAT1 was proprietary to the manufacturer, the geometry and knowledge of conventional MLI systems should

allow for a reasonable estimate. Conventional MLI systems consist of a tightly packed, alternating layers of reflectors and spacers contained within the vacuum space of the Dewar. The vacuum removes convection as a heat transfer mode through the MLI, the spacers are made of low conductivity materials which minimize conduction, and the reflectors reduce radiation. The analysis in this section will therefore calculate the heat transfer through the MLI of the conventional Dewar in a radiation only environment. To support this analysis, a supplemental calculation was done using the Lockheed Equation, an empirically derived formula for heat transfer through an MLI system which accounts for conductions.

The total heat gain through the conventional MLI was calculated using a radiative resistance network. For the resistance network, each radiation shield has three resistive components, the resistance to absorption, resistance to emission, and the view factor to the next shield, shown in Figure 3-9. Assuming a gray body, and applying of Kirchhoff's law, the absorptivity of each shield was equal to the emissivity. From the radiative resistance model, the total heat transfer into the Dewar is calculated from equations (3-3) and (3-4):

$$q = \frac{\sigma(T_{inner\ wall}^4 - T_{outer\ wall}^4)}{R_{total}} \tag{3-3}$$

$$R_{total} = \sum_{i=1}^{50} R_i \ \ where\ R_i = \frac{1-\varepsilon}{\varepsilon A_i} + \frac{1}{A_i} + \frac{1-\varepsilon}{\varepsilon A_{i+1}} \tag{3-4}$$

In equation (3-3), q is the net heat exchange between the inner and outer wall, σ is the Stefan Boltzmann constant, T is the temperature of each wall, and R_{total} is the total radiative resistance, calculated in equation (3-4). In equation (3-4), ε is the emissivity of the radiation shields and A_i is the surface area of the shields. The view

factor, F, does not appear in the second resistive term when the radiation is calculated from the inner wall, out, as the view factor will always be equal to one. From equation (3-4), the resistance of the MLI system is the summation of the three resistance terms of each shield.

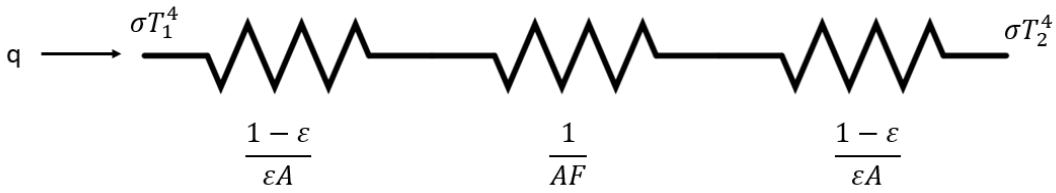

Figure 3-9: The radiation resistance network between two surfaces

For the calculation of the heat transfer through the MLI of the conventional bucket Dewar, the constants and emissivity used were those developed for double-sided aluminized Mylar, also referred to simply as aluminized Mylar. The model treated the 50 mm space for insulation as containing 50 layers of aluminized Mylar. The last piece of the calculation was the boundary temperatures to the MLI. As a conservative estimate, the inner boundary, the bucket, was held at 2 K. The outer boundary was the estimated temperature of the outer wall of the bucket Dewar. This data was not recorded during the flight and will instead be determined from the literature. NASA provides a model for the properties of the atmosphere with altitude, which determines that the temperature at 39.7 km is 261 K [25]. As discussed in Chapter 2, the outer walls of the Dewar can be expected to be 20-40 K warmer than the atmosphere, which will depend on the weather, time of day, and other factors. As such, this calculation will be performed from the range of 230-300 K, which includes potential outer wall temperatures from lower altitudes. This calculation is shown in Figure 3-10, which shows that even for a temperature difference of 40 K between the outer wall and

atmosphere, the heat transfer through the MLI will not reach 10% of the total heat transfer to the superfluid helium. Accordingly, while the MLI system may have contained more than 50 layers of radiation shielding, this would produce minimal benefits to the total heat transfer.

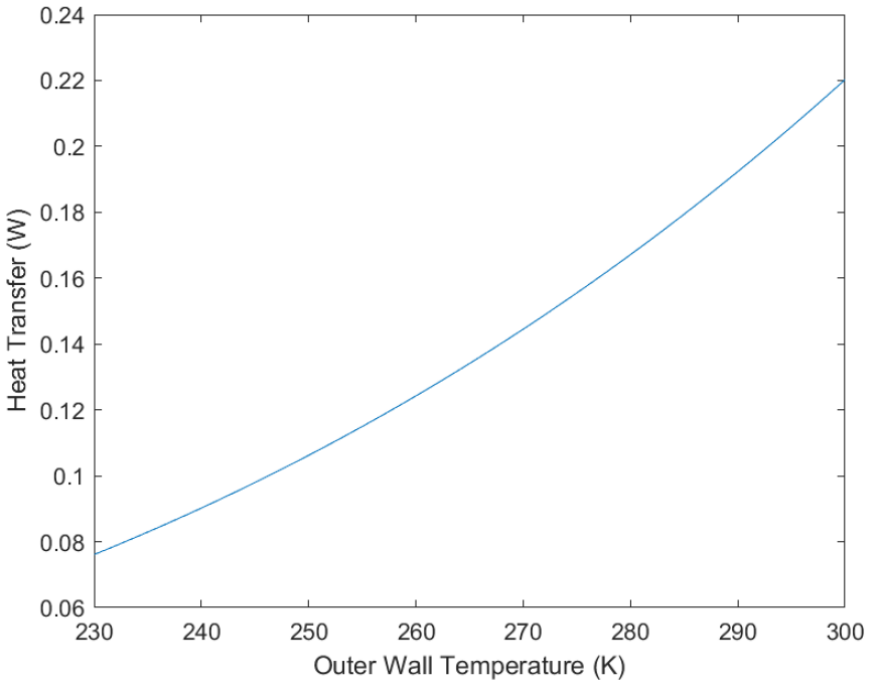

Figure 3-10: Estimate of the heat transfer through the BOBCAT-1 MLI with variable outer wall temperature

As mentioned previously, the results presented in Figure 3-10 are supported by an additional model making use of the Lockheed Equation, equation (3-5) [26].

$$q'' = \frac{C_s \overline{N^{3.56}} T_m}{N_s + 1}(T_H - T_c) + \frac{C_r \varepsilon_{tr}}{N_s}(T_H^{4.67} - T_c^{4.67}) \qquad (3\text{-}5)$$

The Lockheed Equation is an established analytical tool for MLI systems. It is an empirically derived equation that captures both the radiation and conduction through conventional MLI systems. In equation (3-3), C_s and C_r are empirically determined constants, N_s refers to the number of shields, $\overline{N}$ refers number of shields per centimeter, ε_{tr} is the emissivity, and T_H, T_C, and T_m refer to the temperature of the hot side, cold

side, and average of the two. This analysis again assumes that there are 50 radiation shields made of aluminized Mylar with 10 radiation shields per centimeter. Using the same boundary conditions from the previous model, Figure 3-11 presents the results of the Lockheed Equation with the ideal MLI analysis from Figure 3-10, showing that the assumption of a radiation only environment was a reasonable one.

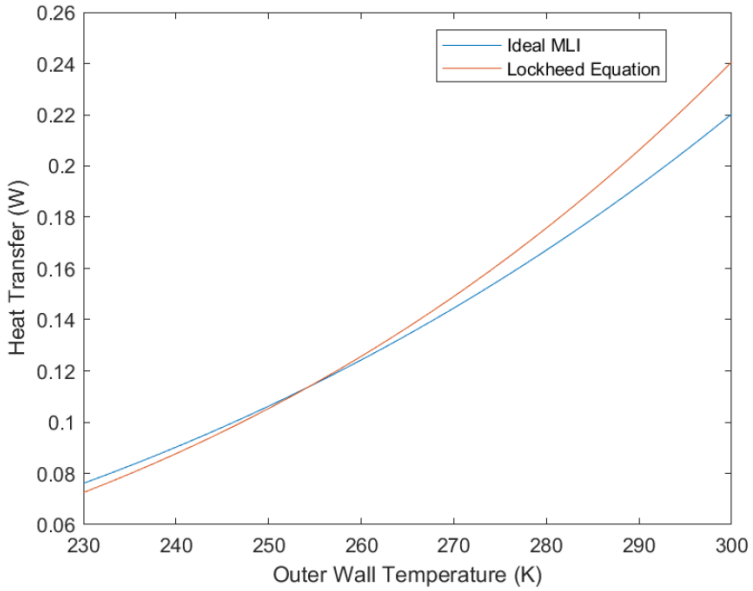

Figure 3-11: Comparison of the ideal MLI and Lockheed Equation models of the BOBCAT-1 MLI heat transfer

To conclude on BOBCAT-1, the cryogen transfer process and boiloff experiments were successful. Of the 2.8 W that reached the superfluid helium in the Dewar, corrected for the generation by the level sensors, the vast majority was due to conduction down the walls and insert of the bucket. As the open aperture provides limits on the effectiveness of the Dewar, this value is 2.8 W is nearly the lower limit for the design of a bucket Dewar of these dimensions. The total heat transfer to the superfluid helium, and the portion due to the heat transfer through the MLI, will serve as a valuable baseline for comparisons to the BOBCAT-2 ultra-light Dewar.

Chapter 4 BOBCAT-2 Design and Assembly

The BOBCAT-2 mission will be the first to fly the ultra-light Dewar concept described within this thesis. In order to maximize the comparability of the conventional bucket Dewar of BOBCAT-1 to the ultra-light Dewar, the designs were constrained to be as similar as possible. The initial designs of the ultra-light Dewar, completed prior to this thesis, are presented in Section 4.1. The two most important aspects of the ultra-light Dewar are the thin-walled vessel and the novel MLI system within the vacuum space of the vessel. The thin-walled design involved long welds of thin metals, and a prototype was necessary to confirm manufacturability prior to approving the flight version. The MLI system was designed with both efficient insulation and ease of assembly in mind. Verifying the novel MLI concept involved a second prototype to confirm it could be assembled. Both prototypes are discussed in Section 4.2. Section 4.3 then presents the assembly of the ultra-light Dewar for the flight of BOBCAT-2.

Section 4.1: BOBCAT-2 Prior Work

While the launch of BOBCAT-1 was not until the fall of 2019, work on the BOBCAT-2 payload began prior to this flight. Before the starting point for the new work in this thesis, the concept for the ultra-light Dewar was proposed, and the initial designs were made. These initial designs informed the team on expected difficulties in manufacturing and assembling the ultra-light Dewar. As the prior work on BOBCAT-2 is introduced here, many of the anticipated difficulties will be presented as well.

The ultra-light Dewar design for BOBCAT-2 included a bucket of the same dimensions as the conventional Dewar from BOBCAT-1, to maximize the similarity of

the experiments. The walls of the bucket and vacuum space were designed with awareness of the vendor's capabilities and recommendations, and the smallest reasonable wall thickness, 0.6mm, was used. An external and an internal view of this thin-walled vessel is shown in Figure 4-1 and Figure 4-2. The vessel is created with long vertical weld seams that must be leak tight, so checks on the vacuum integrity are vital. This vessel was made of four key components, the outer and inner walls, the bottom end, and the annulus, or the lid to the vacuum space (not the bucket). Welded to the annulus are two vent elbows which lead into to the vacuum space. At each joint between the components of the vessel, the vessel is sealed by high aspect ratio indium seals, which were first described by Knudsen [27]. Indium is a soft, ductile metal that acts as the gasket in the seal. When compressed between the shell and the bottom end or the annulus, indium deforms to fill any scratches or gaps and cold-welds to the surfaces, creating a highly effective vacuum seal.

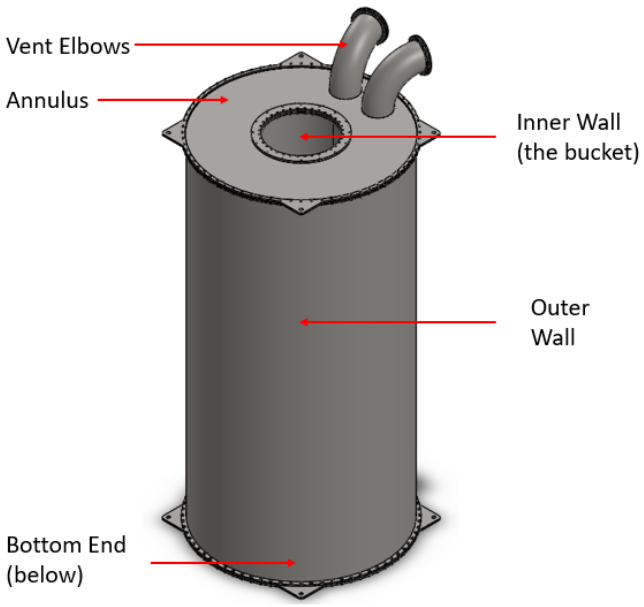

Figure 4-1: External view of the design of the ultra-light Dewar for BOBCAT-2

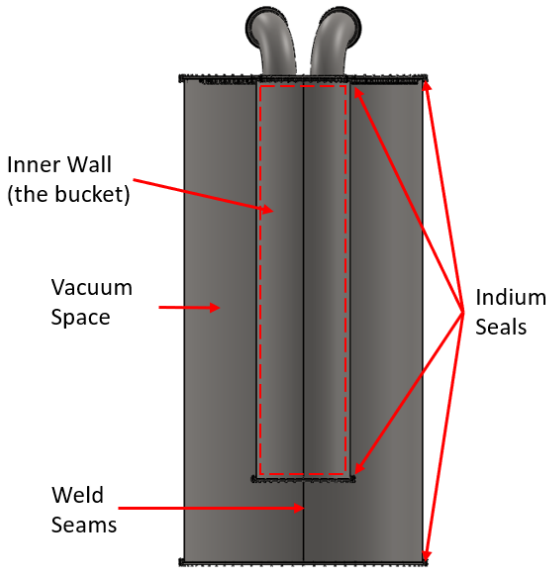

Figure 4-2: Internal view of the vacuum space and bucket of the ultra-light Dewar

The thin-walled design of the ultra-light Dewar necessitated a novel MLI system, and much of the designs revolve around constructing an efficient MLI system that allows for air to flow out on ascent. The MLI is contained within the vacuum space of the Dewar. As discussed in Section 2.2, venting conventional MLI can take up to 50 hours, yet the ascent time for ballooning missions is often 2-3 hours. Therefore, the ultra-light Dewar MLI cannot be constructed as one "blanket" of multiple layers of reflectors and spacers and must be made such that it provides space for the air to vent. Additionally, the MLI must be rigid enough to prevent contact between the layers, which would act as a thermal short. The MLI therefore consists of two main parts, the fourteen shields for the side and bottom of the bucket, and the insulation below the annulus, which acts as a thermal closeout. The shields are made from double-sided aluminized Mylar sheets wrapped around hoops which are suspended and anchored with Kevlar strings. A system of springs is used to keep the shields in their proper locations, 1.6 cm apart radially, by maintaining tension on the Kevlar. This spacing is

much larger than conventional MLI, and it was made to allow air to vent out on ascent. On the bottom face of each shield is a circular "drumhead" of aluminized Mylar adhered to the bottom hoop. The vertically-wrapped sheets and the drumheads form a system of concentric shields building out from the cryogenic bucket, shown in Figure 4-3. Figure 4-3 also shows the vent path of air while the payload ascends.

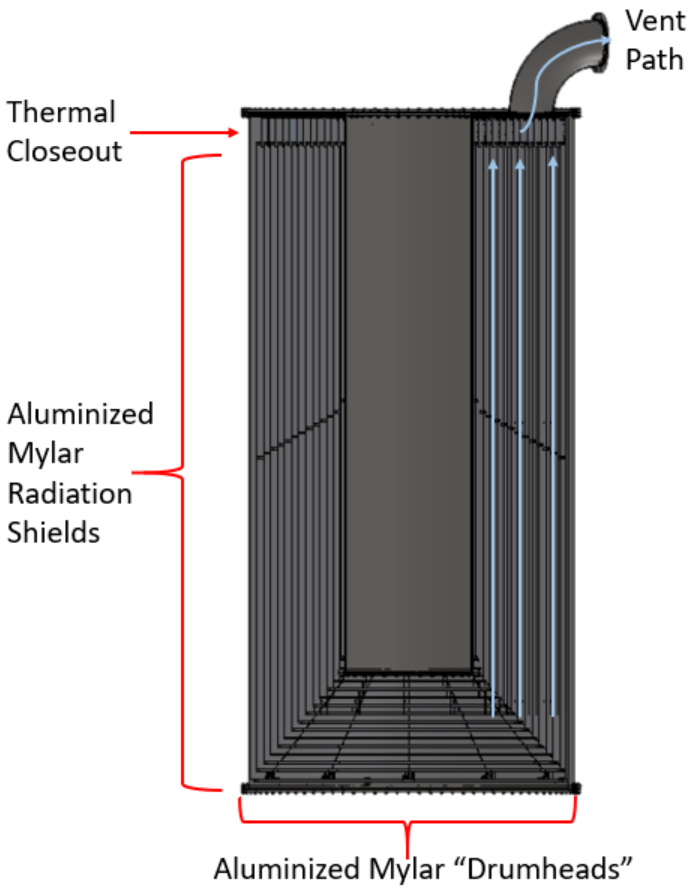

Figure 4-3: Cross-section of the ultra-light Dewar with insulation shown and annotated

The last portion of the MLI system is thermal closeout under the annulus. The annulus serves as the mounting location for the shields and includes the vent lines that allow the air to vent on ascent, but it must also minimize heat transfer entering the MLI from above. The relationship between allowing air to vent while blocking conduction

and radiation leads to the selected design. A close-up of the initial design of the components under the annulus is shown in Figure 4-4. Welded to the annulus are the mounting components for the shields, which consist of twelve mounting locations per shield, equally spaced radially. The springs that hold the vertical Kevlar strings are attached here, as well as twelve layers of small, rolled aluminum shields which help to block radiation radially. Lastly, horizontal to the vessel are four layers of aluminum axial baffles to reduce radiation downwards from the annulus. A schematic of the layers of aluminum baffles is shown in Figure 4-5.

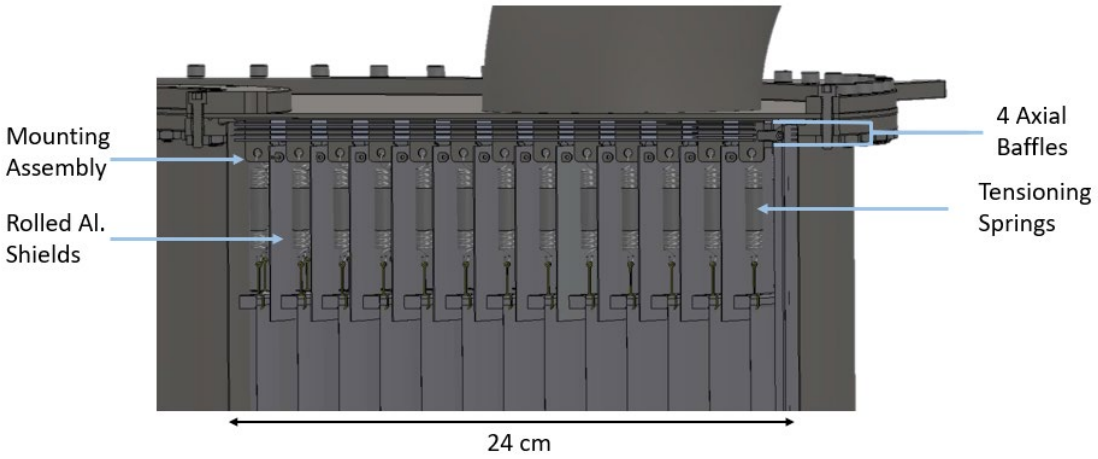

Figure 4-4: Close-up cross-section showing the insulation assembly below the annulus

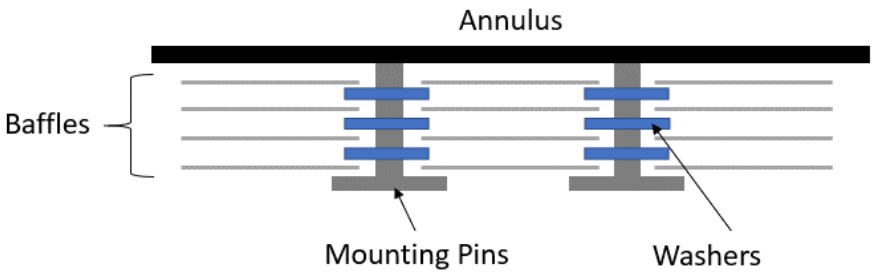

Figure 4-5: Schematic of the baffle buildup below the annulus

Section 4.2: Ultra-Light Dewar Prototypes

Before finalizing the designs and beginning production of the ultra-light Dewar for the BOBCAT-2 flight, two prototypes were constructed. The first prototype was the fabrication practice unit that was ordered from the vendor who manufactured the vacuum shell. The prototype was ordered to ensure that the thin-walled vessel could be machined, rolled, and welded as specified. The second prototype was a small-scale version of the MLI concept of the ultra-light Dewar. It was constructed to answer outlying questions regarding assembling the radiation shields. A detailed discussion of the MLI assembly process will be discussed while discussing this prototype.

Section 4.2.1: The Fabrication Practice Unit

The fabrication practice unit was ordered to confirm a thin-walled, cryogenic vessel could be manufactured to the desired specifications. This prototype was manufactured according to the dimensions of the bucket of the BOBCAT-1 and BOBCAT-2 Dewars – 1.2 m tall with a diameter of 25 cm and a thickness of 0.6 mm. The fabrication practice unit is shown in Figure 4-6. The vessel included one indium seal on each end of the cylinder and connections to perform a leak test.

Figure 4-6: Fabrication practice unit, weld seam up

Once a visual inspection of the welds was completed, the vessel was setup for a leak test. As the thin-walled construction is not intended to survive a 101 kPa pressure

gradient, that from ambient pressure to a vacuum at sea-level, the vessel was leak tested with a slight (6.9 kPa) overpressure. First, the two indium seals were created. Then, the 6.9 kPa overpressure of helium was pumped into the vessel, and a leak checker in "sniff mode" was swept along the outside of the vessel to detect helium. No discernable leaks were detected along the weld or seals; therefore, the vessel was determined to be leak tight.

Section 4.2.2: The Assembly Prototype

The second prototype, the assembly prototype, was designed to practice the assembly of the MLI concept of the ultra-light Dewar and determine the best way to build the radiation shields. As mentioned previously, the radiation shields of the MLI act as concentric shields, building outwards from the bucket of the Dewar. Each of these shields includes a frame of aluminum hoops suspended by Kevlar string to anchor the shield in position. This frame is then wrapped in aluminized Mylar on the side and bottom. The idea behind the shields can be seen in Figure 4-7, which shows the "drumhead" or bottom of each shield and one Kevlar and aluminum hoop frame. The drumhead is made with one aluminum hoop with aluminized Mylar attached. Not shown in this figure is the aluminized Mylar sheet that would be wrapped around the hoops vertically to create a complete shield. The radial spacing of the shields for the prototype was the same as the flight version of the Dewar, 1.6cm. While the spacing was selected to allow air to vent, it is also important to keep the individual shields from touching, which would create a thermal short in the MLI.

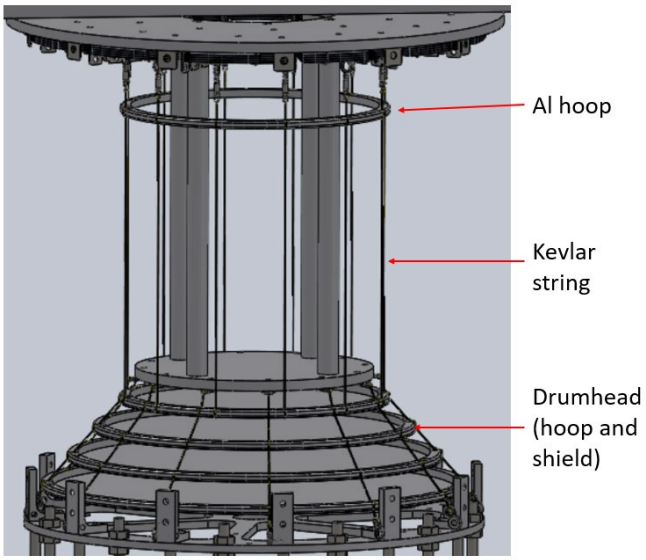

Figure 4-7: The frame of the innermost shield without wrapped aluminized Mylar

The assembly of the prototype proceeded in a similar manner to the planned assembly of the ultra-light Dewar. First, a gantry, or frame, was constructed to hold the assembly while building it down from the annulus. Next, mounting components and axial baffles were attached to the annulus, as seen in Figure 4-8. For the prototype, the mounting components were bolted to the annulus, while they were welded for the flight vessel. The axial baffles were then attached. Each baffle visible in Figure 4-8 is a stack of four baffles spaced by small washers to provide radiation shielding with minimal contact. Pins through the mounting components for the baffles hold them in place. With this annulus assembly built, it was attached to the gantry to begin building the shields.

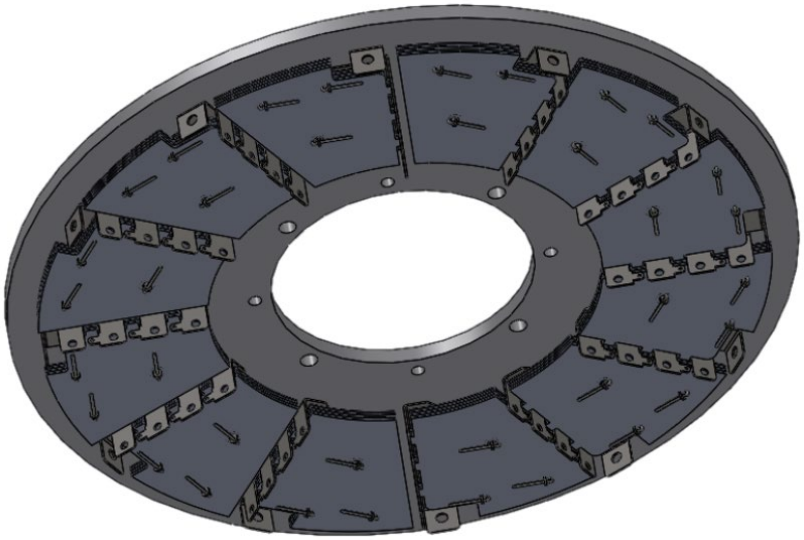

Figure 4-8: Prototype annulus with mounting components and axial baffles attached

The assembly of the shields began by positioning the drumheads and tying them in place using Kevlar and special fixtures. Figure 4-9 shows the assembled drumheads, tied to components attached to the bottom of the mock inner and outer walls. The hoops have smooth holes in them for tying the Kevlar to the hoops. It was determined that the best way to anchor the drumheads was by tying a knot to each of the drumheads successively by size. When the drumheads were tied at each end to components of the inner and outer walls, and this was repeated twelve times radially, the drumheads were held firmly in place.

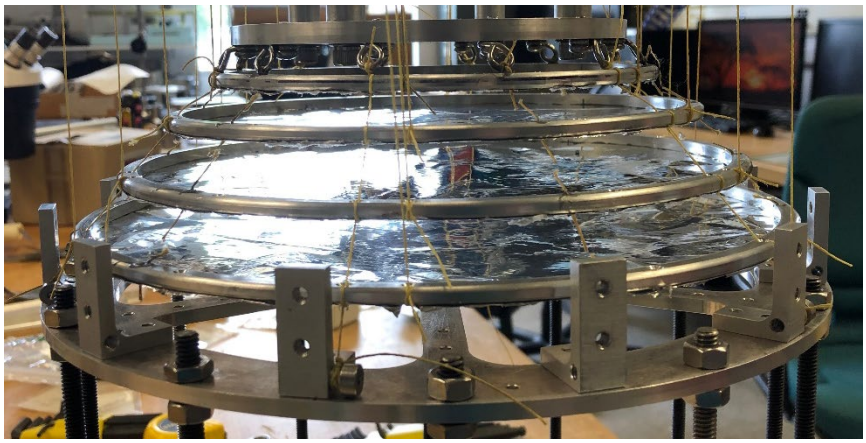

Figure 4-9: Drumheads and Kevlar strings of the assembly prototype

With the drumheads anchored in the proper positions, they serve as the bottom tie-off for the vertical strings, while the springs attached to the annulus mounting components are the top tie-off. These vertical strings were then tied, positioning an additional hoop near the annulus, creating the frame of the radiation shield. Each shield was then finished by taping aluminized Mylar to the top hoop and the drumhead. These steps are shown in Figure 4-10.

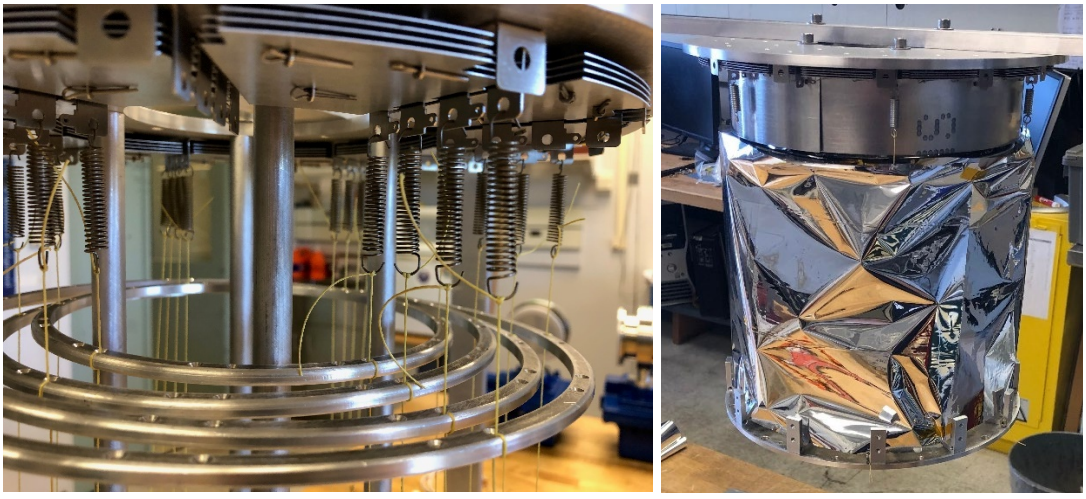

Figure 4-10: BOBCAT-2 assembly prototype left) without aluminized Mylar shield and right) with aluminized Mylar shield

There were several important findings from the prototype that led to design or assembly process changes for the full-scale ultra-light Dewar. First, the springs in the initial design of the payload were undersized for the 7N of force that was applied to hold the shields taut. For the assembly of the prototype, new springs were purchased that were adequately sized to handle the load, but also to extend a reasonable length under this load. This ensured that when tying the Kevlar to the springs by hand, small changes in extension length did not lead to vastly different tensions between different springs. Additionally, the manner of tying the knots, and the components of the tie-offs, were selected for easy assembly that maintains tension in the shield frames. Lastly, the small-scale assembly prototype was used to determine the best way to adhere the Mylar sheets to the frame of the shields. From practice and theory, aluminized Mylar tape was selected because the adhesive is known to survive cryogenic temperatures, it does not diminish the emissive properties of the Mylar sheets, and the option of cryogenic epoxy required 8 hours to set and would have added appreciable thermal mass to the system. Furthermore, the aluminized Mylar tape was not as permanent as the epoxy and could be disassembled or adjusted if necessary.

Section 4.3: Ultra-light Dewar design and assembly

After the prototypes were built and the designs of the ultra-light Dewar were finalized, the parts for the flight Dewar were ordered or made, and assembly began. There were two portions to the assembly process – the assembly work on the ultra-light Dewar, including the vacuum vessel and MLI system, and the assembly of the full BOBCAT-2 payload by mounting the ultra-light Dewar to the flight gondola and attaching the fluid and electrical components. The ultra-light Dewar assembly will be

discussed in Section 4.3.1, while integration with the full flight payload will be discussed in Section 4.3.2

Section 4.3.1: Ultra-Light Dewar Assembly

The steps to create the BOBCAT-2 ultra-light Dewar started with the arrival of the vacuum shell. The vacuum shell consists of the stainless steel components that create the Dewar bucket and the vacuum space, as was shown in Figure 4-1 and Figure 4-2. The vendor supplied the results from an in-house leak check that reported high vacuum integrity of 10^{-9} cm^3s^{-1}. The vessel was checked at NASA GSFC to verify the integrity of the vessel. This test determined that the vessel had two detectable leaks at weld locations on the vessel, so it was shipped to a local welder for repair. It was concluded that due to the fragile nature of the thin-walled vessel, it was damaged during transport to NASA GSFC. As the full BOBCAT-2 payload will be transported to the field for launch, vibration isolators were added to the payload to mitigate this problem in the future. Once the leak test was rerun, it was determined that the leaks were adequately repaired, and assembly could begin.

The first assembly step was to create the gantry, a structure used strictly for the assembly of the ultra-light Dewar. At the same time, the drumheads were created from an aluminum hoop of each size, aluminized Mylar, and cryogenic epoxy. Assembly then proceeded with the creation of the baffle layers below the annulus. Welded to the annulus were twelve radially symmetric mounting components which have tabs for attaching the baffles and springs. The baffles were assembled in the same way as in the assembly prototype, as shown in Figure 4-11. At this point, two indium seals were created. First, the vertical portion and the bottom end of the inner wall were sealed

together, creating the bucket of the Dewar. Then, the annulus was connected to the inner wall of the Dewar. Once these portions were assembled, the bulk assembly of the MLI began.

Figure 4-11: Annulus of the ultra-light Dewar with baffles installed

The remainder of the MLI assembly was conducted with the annulus and inner wall attached to the gantry. Suspending the assembly was critical to building the MLI down from the annulus. The annulus and inner wall attached to the gantry is shown in Figure 4-12. Due to the thin construction of the annulus (1.6mm), support for the vent elbows was added to the gantry to minimize the loading due to their weight. Figure 4-13 shows warpage of the annulus from repeated assembly and disassembly of the vacuum shell for leak checking and weld repair. Despite the visible warpage, the final leak check showed that the compression of the annulus between the outer wall flange below and the compression ring above removed the warpage and created a tight seal.

Figure 4-12: Annulus and inner wall suspended from the gantry with elbow support structure

Figure 4-13: Annulus warpage between the compression ring and the wall flange

The key to building frames of each radiation shield was to maintain tension while assembling. To do so, a positioning fixture for the drumheads was assembled from the floor of the gantry. This component was locked in the proper position by rods

and locking nuts from the floor of the gantry. When the vertical positioning bars (shown in Figure 4-14) were removed, there were two parts to the flight vessel locked in the correct positions.

Figure 4-14: Inner wall of the ultra-light Dewar with the vertical bars positioning the drumhead positioning fixture mounted to the proper location

The next step was to assemble the drumheads in the correct positions by using six radial spacing fixtures while tying the Kevlar. The drumheads held in the correct position by the spacing fixtures is shown in Figure 4-15.

Figure 4-15: Spacing fixtures holding the drumheads in the proper location

Once the drumheads were tied in place with the Kevlar string, the assembly of the vertical shields began. In order to assemble the radiation shields, a length of Kevlar string was tied to a spring, and the spring was attached to the proper mounting location from the annulus. The Kevlar was then tied to two aluminum hoops, one just below the spring, and one halfway downwards to the drumhead. This was repeated twelve times radially, which produced the completed frame of a radiation shield. A view of this assembly below the annulus is shown in Figure 4-16.

Figure 4-16: Springs and Kevlar held in tension between the annulus and the drumhead (not shown)

With the Kevlar and hoops held in their proper locations, a sheet of aluminized Mylar, cut to the proper dimensions, was wrapped around the hoops and taped in place with aluminized Mylar tape. Before the next shield was added, the rolled aluminum shields were attached below the annulus to aid in blocking the radiation as a part of the thermal closeout. These steps were to be repeated for each of the shields until the MLI system was complete. An image from the completed second layer of radiation shielding is shown in Figure 4-17. The assembly work on the MLI system was the final step on design and assembly performed for this thesis, and future work will be discussed for the remainder of this chapter and in Chapter 6.

Figure 4-17: Completed radiation shield with the frame of the next shield

Section 4.3.2: Integration of the Ultra-Light Dewar and the BOBCAT-2 Payload

Following the assembly of the MLI system for the ultra-light Dewar, the next steps create a vacuum tight vessel and integrate it with the full BOBCAT-2 payload. Sealing the MLI system within the outer wall of the Dewar and integrating the ultra-light Dewar with the full BOBCAT-2 payload were not completed for this thesis and will be completed when deployment to the launch site is nearer.

Integrating the ultra-light Dewar involves mechanical, fluid, and electrical integration. Mechanically, the eight large bolt holes, four on top and four on bottom (shown in Figure 4-1), serve as the main connections to the larger gondola, which was

designed and assembled by other members of the BOBCAT team. From a fluid perspective, the connections to the ultra-light Dewar include the insert from the BOBCAT-1 conventional bucket Dewar, shown schematically in Figure 3-2. Additionally, pressure sensors, motor valves, and electrical connections will be attached to the vent elbows. These attachments to the vent elbows include two relief valves, the pressure sensors, and the connection port for the instrumentation in the MLI assembly. This instrumentation will be discussed at length in Section 5.3, following the thermal analysis of the MLI. Also connected to the vent elbow are the motorized valves which are used to seal the vessel at float. The fully integrated gondola is shown in Figure 4-18.

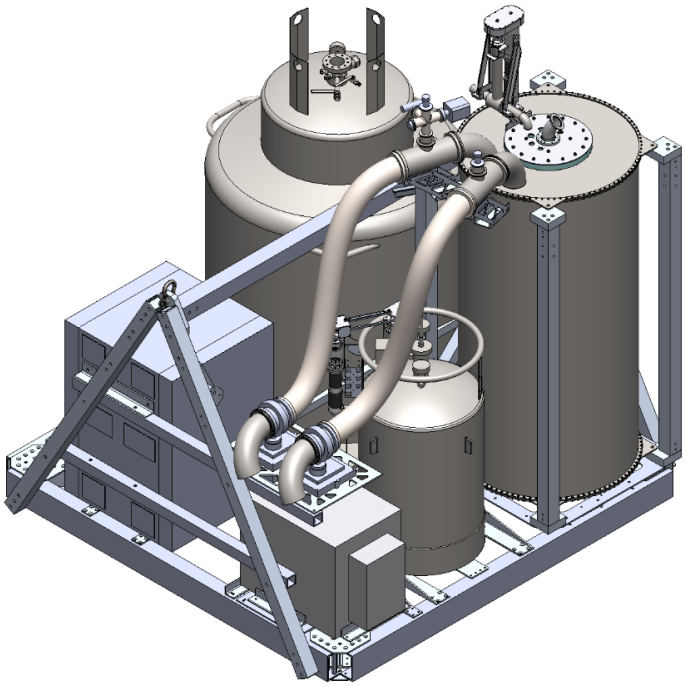

Figure 4-18: The integrated BOBCAT-2 payload

Chapter 5 BOBCAT-2 Thermal and Fluid Analyses

The thin-walled design of the ultra-light Dewar concept necessitated significant changes to the MLI system which insulates the bucket. In order to validate this concept, a fluid model was developed to show the air can vent from the MLI as the payload ascends, shown in Section 5.1. Additionally, a thermal model was developed to determine the anticipated thermal performance of the ultra-light Dewar concept, which will be presented in Section 5.2. This model serves to outline expected performance prior to the flight, and when integrated with flight data after, demonstrate the BOBCAT team's understanding of the thermal environment encountered by the Dewar. Section 5.3 will then discuss the instrumentation scheme for the ultra-light Dewar to return the flight data of interest.

Section 5.1: Ultra-Light Dewar Fluid Model

In order to achieve the thin-walled design of the BOBCAT-2 ultra-light Dewar, the Dewar must vent the vacuum space on ascent and only create a vacuum at float altitude. This venting is not a controlled process, but one that is expected to occur naturally on ascent, due to pressure difference between the inside of the vacuum space and the outside atmosphere. This pressure differential will induce flow out of the vacuum space but must do so without creating a pressure gradient large enough to damage the thin-walled Dewar. The calculations in Section 5.1.1 will show that the pressure buildup is expected to be negligible compared to the yield stress of the ultra-light Dewar. After the vessel has reached float altitude and the venting has stopped, the vessel will be sealed, and the cryogen transfer operations will be performed. The expected volume of cryogen needed is calculated in Section 5.1.2.

Section 5.1.1: Dewar Venting on Ascent

Conventional cryogenic Dewars do not have the ability to vent the insulation space, and therefore have thick walls to withstand a pressure difference of 101 kPa at sea-level. The ultra-light Dewar concept does not create a vacuum until float altitude (upwards of 24 km) is achieved, where the maximum pressure difference would be around 3 kPa. This enabled the walls of the ultra-light Dewar to be manufactured 0.6 mm thick. The yield stress of the ultra-light Dewar walls, made of stainless steel 304, is 215 MPa, as reported by MatWeb [28]. The stress within a pressure vessel can be calculated from the hoop stress equation, equation (5-1):

$$\sigma_{hoop} = \frac{Pr}{t} \tag{5-1}$$

From equation (5-1), P is the pressure difference from the outside to the inside of the vessel, r is the radius of the cylinder, and t is the wall thickness. For the ultra-light Dewar, the radius of the outer wall is 0.38 m. At sea-level, the ultra-light Dewar would experience a hoop stress of 64 MPa. At 24 km, the minimum float altitude, it would only experience a hoop stress of 1.87 MPa based on an atmospheric pressure of 2940 Pa.

While the hoop stress for the ultra-light Dewar at sea-level would not exceed the yield stress for the vessel, this level of stress would still pose a risk to the vessel, especially with the delicate, 1.5-meter long weld seams. As such, this vessel will not be depressurized anywhere other than on the gondola at float altitude. The stress experienced at float altitude is then almost 30-100 times less, depending on the float altitude achieved. With the incident stress from atmospheric pressure in the

environments of sea-level and float altitude determined, additional analysis involves the pressure incident on the vessel as it ascends to float altitude.

To determine any potential for a substantial pressure gradient to build in the vessel as it ascends to float altitude, a control volume analysis of the air flow out of the vacuum space was performed. This analysis focused on determining the necessary pressure difference from top to bottom of the vacuum shell to force flow through the MLI system. The equality used for this analysis was that the mass flow rate out of the vessel was equal to the rate of change of the density of the atmosphere on ascent.

The ascent rate of the payload was taken as a linear approximation of the BOBCAT-1 ascent, 39.7 km over 173 minutes, or roughly 4 m/s. With knowledge of the density of the atmosphere with altitude, the ascent rate in meters per second, dh/dt, was translated to a rate of change of density, $d\rho/dh$ of the atmosphere outside of the vessel, in kilogram per cubic meter per meter. NASA provides a simplified, piecewise function of air properties with altitude [25]. A graphical representation of these properties is shown in Figure 5-1 [29]. The rate of change of density per meter of altitude was then translated to the volumetric flow rate in cubic meters per second, $\dot{V}$, of air out of the vessel by dividing by the density of air, ρ, at each altitude and multiplying by the volume, V, of the vessel. The full equation, equation (5-2), is shown below.

$$\dot{V} * \rho = \frac{d\rho}{dh} * \frac{dh}{dt} * V \tag{5-2}$$

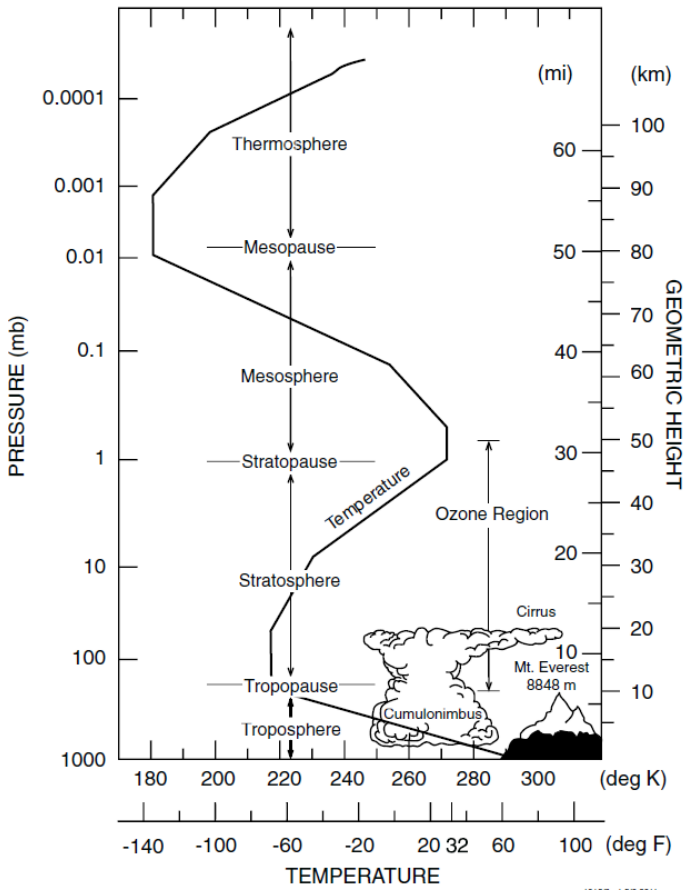

Figure 5-1: Atmospheric properties with altitude [29]

After the necessary volumetric flow rate per altitude was determined, it was equated to the volumetric flow rate out of the vessel as a function of the pressure difference. The pressure difference was then the only unknown of the system, and the equations could be solved. The MLI in the vacuum space was modelled as fourteen strictly vertical annular channels, 1.46m in length. Each channel was treated as an independent fluid flow problem with the vertical pressure gradient assumed equal across each channel. The Navier Stokes equation for the cylindrical coordinates is shown in equation (5-3), where in addition to the variables from equation (5-2), g is the gravitational constant, μ is the viscosity, and r, θ, and z are the coordinate system.

$$\rho\left(\frac{dv_z}{dt}+v_r\frac{dv_z}{dr}+\frac{v_\theta}{r}\frac{dv_z}{d\theta}+v_z\frac{dv_z}{dz}\right) = \rho g-\frac{dp}{dz}+\mu[\frac{1}{r}\frac{d}{dr}\left(r\frac{dv_z}{dr}\right)+\frac{1}{r^2}\frac{d^2v_z}{d\theta^2}+\frac{d^2v_z}{dz^2}] \quad (5\text{-}3)$$

Equation (5-3) reduces to equation (5-4) with the assumptions of incompressible one-dimensional flow in the z direction:

$$0 = \rho g-\frac{dp}{dz}+\mu[\frac{1}{r}\frac{d}{dr}\left(r\frac{dv_z}{dr}\right)] \quad (5\text{-}4)$$

The differential equation (5-4) was solved with the boundary conditions that the velocity at the wall of each annular channel is zero, shown in equation (5-5):

$$\frac{1}{\mu}\left(\frac{dp}{dz}-\rho g\right)=\left[\frac{1}{r}\frac{d}{dr}\left(r\frac{dv_z}{dr}\right)\right], where\ v_z(r_i)=v_z(r_o)=0 \quad (5\text{-}5)$$

The solution to the equation is therefore equation (5-6):

$$v_z(r)=\frac{1}{4\mu}\left(\rho g-\frac{dp}{dz}\right)[\frac{\ln\left(\frac{r}{r_i}\right)}{\ln\left(\frac{r_o}{r_i}\right)}(r_o^2-r_i^2)-(r^2-r_i^2)] \quad (5\text{-}6)$$

From equation (5-6), r_o and r_i were updated for each of the fourteen shield radii. Equation (5-6) was then integrated for volumetric flow rate to become equation (5-7), the volumetric flow for each channel:

$$\dot{V} = \int_{r_i}^{r_o} v_z 2\pi r dr \quad (5\text{-}7)$$

MATLAB was used to sum the flow rate for each annular channel and solve for the pressure gradient at discrete altitudes to equate equation (5-1) to equation (5-7). As can be seen in Figure 5-2, the maximum pressure gradient developed, which is at sea level, is less than 18 Pa, which is negligible compared to the pressure of the atmosphere. This equals a hoop stress of 22.8 kPa. At 40 km, the pressure difference is 65 mPa, again much less than the ambient 300 Pa.

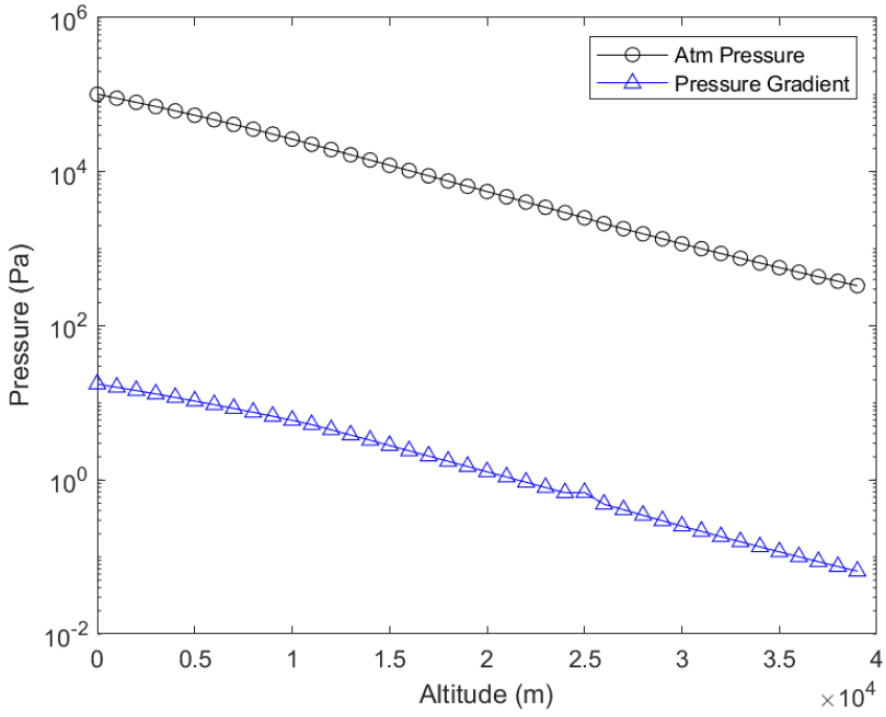

Figure 5-2: Comparison of the atmospheric pressure to the pressure gradient within the ultra-light Dewar on ascent

Despite the excellent performance of venting in the MLI, additional considerations were made for venting the air from the vacuum space on ascent. The flow was difficult to model in the thermal closeout assembly below the annulus, previously shown in Figure 4-4. Considering the minimal flow resistance of the proceeding calculations, an assumption was made that if the cross-sectional area at choke points was not considerably less than the 0.1-meter diameter (80 cm^2) elbows, the air would be able to escape without a significant pressure difference.

The initial design of the payload only afforded 2 mm of spacing between the baffle nearest to the annulus and the annulus, which would only allow 6.5 cm^2 of space for the air to vent. Accordingly, holes were added to the baffles in an offset pattern that minimized line of sight paths for radiation into the vessel but added 32 cm^2 of area for venting, as shown in Figure 5-3. The calculations from this section demonstrate that

the ultra-light Dewar will be able to vent on ascent as desired. As a last resort for pressure buildup, two relief valves with 1380 Pa cracking pressures have been installed.

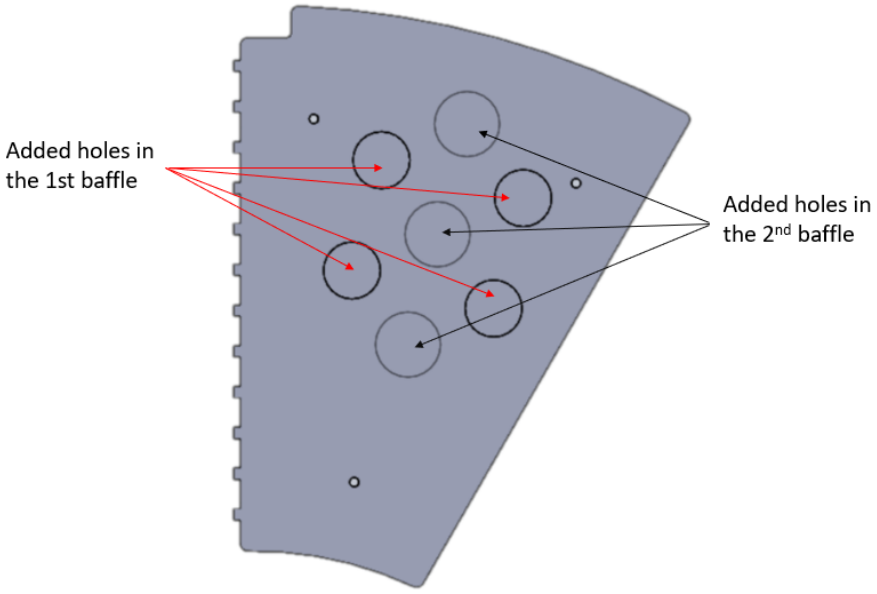

Figure 5-3: Baffle stack with alternating pattern of added holes for extra venting area

Section 5.1.2: Volume of Cryogen Needed for Flight

One additional fluid calculation that was needed for determining the anticipated performance of the ultra-light Dewar was the amount of cryogen required to cool the Dewar and freeze the air in the vacuum space. As opposed to balloon campaigns for astronomical observations, the BOBCAT-1 and BOBCAT-2 flights were technical demonstrations that did not contain telescopes. This reduced the amount of cryogen needed as there was much less mass to cool in the bucket Dewars. This analysis considers the likely case that the BOBCAT-2 payload will fly to 40 km in altitude as BOBCAT-1 did.

The two cryogens used to cool the Dewar are liquid nitrogen and superfluid helium. The liquid nitrogen cools the Dewar to 100 K, and the superfluid helium cools

the Dewar from 100 K to 2 K. The volume of liquid nitrogen needed to cool the ultra-light Dewar was determined using the specific heat and mass of the Dewar components integrated over the 260-100 K temperature range compared with the latent heat of the liquid nitrogen in the storage Dewar (200 kJ/kg) [30]. While this value does not capture the exact behavior of the nitrogen in the Dewar, the latent heat of vaporization should allow for a crude estimate of the volume of cryogen needed. The latent heat of vaporization of helium is 21 kJ/kg, much lower than liquid nitrogen [22]. While the latent heat of vaporization captures the cooling power available in the cryogens, the heat of sublimation will be necessary to determine the volume of cryogen needed to cryoplate the air in the vacuum space onto the inner wall of the Dewar. For nitrogen, the heat of sublimation is 257 kJ/kg, and for oxygen, it is 298 kJ/kg [31].

From this analysis, it will take 2.6 liters (L) of nitrogen to cool the components of the Dewar. It will then take a negligible amount of nitrogen to cool the 570 L of 300 Pa air in the vacuum space for a total of 2.6 L of liquid nitrogen needed for cooling. Due to this low number, the 80 L being flown are many times more than what is necessary. Despite the lower latent heat of vaporization of the liquid helium in the storage Dewar it will only take 0.70 L of liquid helium from the storage Dewar to cool the Dewar because many of the components in the MLI system will equilibrate much warmer than 2 K, as will be shown in the next section. However, for the helium pre-cool, it will need to freeze the remaining air from the vacuum space. This will take 0.77 L of liquid helium for a total of 1.47 L for pre-cooling. The superfluid helium is then the cryogen used to fill the bucket Dewar for the experiment, and 31 L were used

for the BOBCAT-1 flight. Therefore, the 500 L liquid helium storage Dewar is more than enough for the flight of the BOBCAT-2 payload.

Section 5.2: Ultra-Light Dewar Thermal Model

The ultra-light Dewar concept of the BOBCAT-2 mission was designed to reduce the weight of cryogenic Dewars aboard high-altitude balloons while demonstrating adequate thermal performance. Demonstrating thermal performance will be done in two parts – by conducting the flight experiment and comparing the data between BOBCAT-1 and BOBCAT-2, and by developing a thermal model of the ultra-light Dewar establishing expected performance to demonstrate understanding of the thermal environment within this novel Dewar after returning flight data. This section will discuss the development of the pre-flight thermal models and how they compare to the BOBCAT-1 results, as the flight of BOBCAT-2 will occur in fall 2020 or later.

The vent-on-ascent concept of the ultra-light Dewar necessitated an MLI system that minimizes heat transfer into the bucket Dewar without impeding air flow out of the insulation. The Dewar then relies on multiple layers of radiation shielding in a vacuum space in order to insulate the cryogen in the bucket. The vacuum is achieved by cryoplating, as mentioned previously, and the vacuum space surrounding the bucket is used to negate convection as a heat transfer mode inside the Dewar. The MLI is built of highly reflective double-sided aluminized Mylar radiation shields for minimizing radiation. The frame of the radiation shields was made with Kevlar string, which minimizes conduction between the components of the MLI system. Within this section on the thermal analysis of the ultra-light Dewar, Section 5.2.1 will present a thermal model for the radiation between the shields of the MLI. Section 5.2.2 will then consider

the heat transfer through the thermal closeout assembly below the annulus and proceed by integrating these results with the radiation through the shields. Lastly, Section 5.2.3 will discuss the results of these two models and compare them to the results from the BOBCAT-1 analysis.

Section 5.2.1: Heat Transfer Between the Radiation Shields

The model of the heat transfer within the MLI system of the ultra-light Dewar was formulated to capture the potential sources of heat transfer into the bucket while employing simplifying assumptions to ease calculation and provide a model that can be updated with flight data. The relevant components of the MLI for this thermal analysis are shown in a radial slice of the Dewar, Figure 5-4.

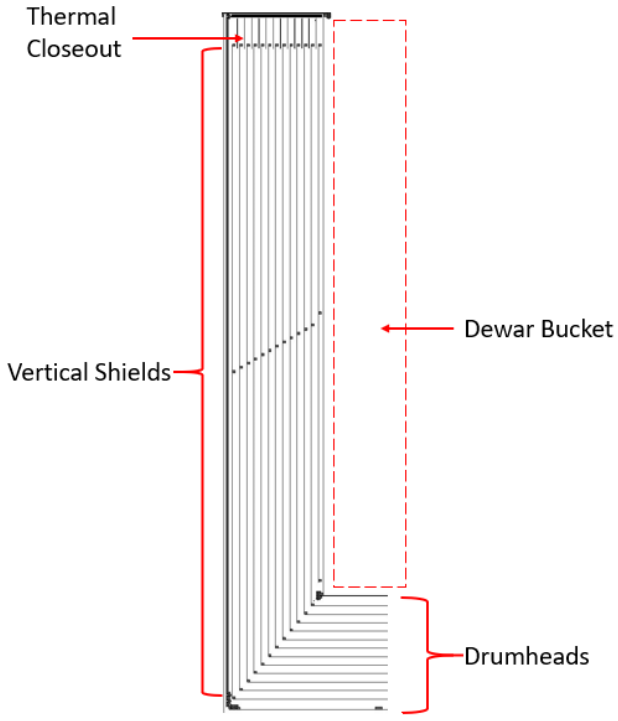

Figure 5-4: Radial slice of the Ultra-Light Dewar MLI

For handling the thermal radiation through the aluminized Mylar components, each wrapped sheet and drumhead shield will be considered as one combined component. Each radiation shield will be treated isothermally from the top of the vertical sheet of aluminized Mylar to the drumhead. The shields will also be assumed to only transfer heat radiatively. First, there is no interstitial material in the novel MLI system, as it affords space for the air to vent on ascent. Additionally, the design of the MLI was such that only Kevlar strings connect the shields to the Dewar mechanically. Using a thermal conductivity of 3 W/m/K [32] with a diameter of 0.6mm, the Kevlar has a thermal conductance on the order of 10^{-6} W/K, which ensures this assumption is accurate. Lastly, due to their large surface area and tight spacing, each radiation shield will be considered to have a radiative view factor of one to the next radiation shield outward.

The total heat gain through the shields was then calculated using a radiative resistance network as developed in Section 3.4. In this resistance network, the boundary conditions were the temperature of the outer wall of the MLI and the temperature of the inner wall, or the bucket of the Dewar. Due to the presence of superfluid helium in the bucket, the inner wall boundary temperature was kept at 2 K. It was shown in BOBCAT-1 that the bucket will develop a vertical temperature gradient for the portion of the bucket above the superfluid helium, yet a due to the low radiative power of materials at low temperatures, the boundary condition of 2 K is not expected to create a significant overestimate of the heat transfer. For the outer boundary, the flight parameters for BOBCAT-2 specify a float altitude above 24 km, where the temperature ranges from 217-261 K, rising monotonically. The anticipated temperature of the

exterior of the payload is then between 230 K and 300 K using the same logic as the BOBCAT-1 analysis.

The relevant thermal properties of the materials in the ultra-light Dewar are shown in Table 5.1. The individual references for each property are included with the value. The emissivity of aluminized Mylar varies between 0.02 and 0.05 with thickness and workmanship [33]. The emissivity of aluminized Mylar reported by the manufacturer was 0.03 and has been revised upwards to 0.04 to account for potential degradation with time. It was assumed that due to the thin (0.233 mm) thickness of the aluminized Mylar, the thermal conductance through each shield radially is sufficiently high to be negligible in this resistive network. The selected boundary temperature of the outer wall for in-depth discussion was 280 K, a best estimate of the outer wall temperature for a float altitude of 40 km. Lastly, selected surface properties of the inner wall were those of stainless steel 304, despite the presence of nitrogen ice plated on its surface. The crystal structure of nitrogen at low pressures is that of a cubic unit cell with a side length of $5.65*10^{-10}$ meters [34]. Based on the low density of air at 40 km, the ice layer on the inner wall would be $4*10^{-6}$ meters thick. The wavelength of thermal radiation at cryogenic temperatures is many times larger than the ice thickness, implying the ice will be transmissive to the radiation in the ultra-light Dewar MLI.

Table 5.1: Conductivity and emissivity of relevant materials

Material	Thermal conductivity	Emissivity
Aluminum 6061	168 (Wm^{-2}) [35]	0.10 [37]
Stainless Steel 304	14.7 (Wm^{-2}) [36]	0.14 [37]

From the properties in Table 5.1, the boundary conditions of the inner and outer wall temperatures of 2 K and 280 K, respectively, and the radiative resistance model detailed in Section 3.4 by equations (3-3) and (3-4), the temperature profile through the shields is shown in Figure 5-5. Based on this temperature profile, the expected heat transfer through the shields is 1.04 W at 280 K. Additional temperature profiles for the 230-300 K range of outer wall boundary conditions are available in Appendix A. The analysis of the thermal performance of the MLI will now proceed to considerations of the heat transfer through the annulus of the vessel.

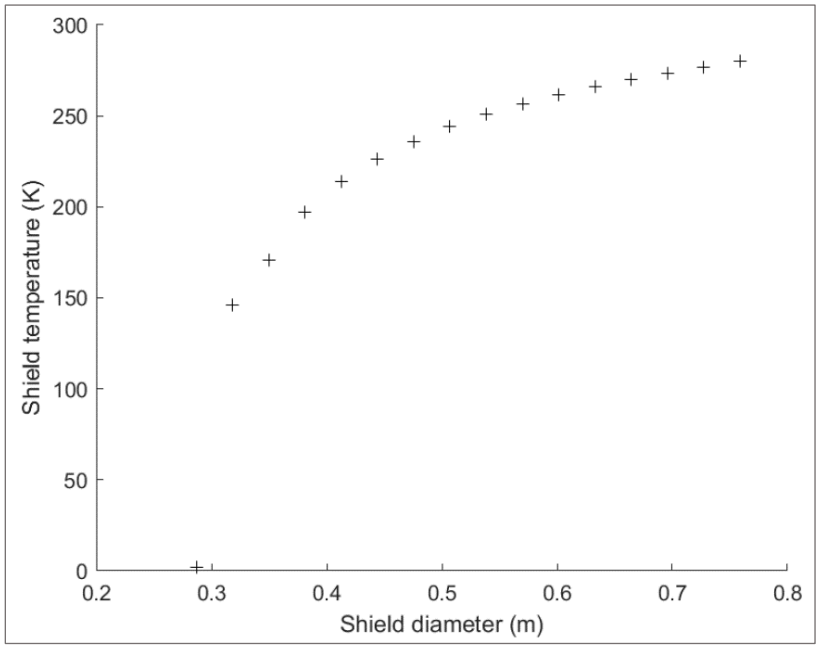

Figure 5-5: Intermediate temperatures within the MLI of the ultra-light Dewar proceeding from the inner wall to the outer wall

Section 5.2.2: Heat Transfer Through the Annulus

The heat transfer through the annulus was considered separately from the vertical shields due to the complications introduced by the geometry and the inclusion of conduction. The assumption of negligible conduction was not valid in the thermal

closeout below the annulus, where increased contact and fewer shields will necessitate consideration of conduction. Figure 5-6 shows a schematic cross section of the assembly below the annulus, which features four radiation-shielding baffles as well as pins to support the baffles from the bottom and washers to separate the baffles. Conduction in the thermal closeout assembly shortcuts some of the baffles by conducting from the annulus, through the pin, and into the bottom baffle. From each heat transfer path, the heat must then radiate from the bottom baffle to enter the larger MLI system.

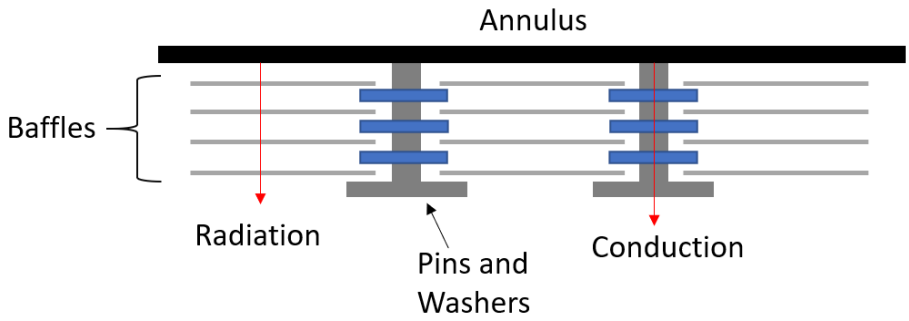

Figure 5-6: Schematic of the mechanical and thermal interactions below the annulus

For this portion of the analysis, there is not an obvious second boundary for the heat transfer equations. The heat transfer will therefore be calculated by varying the temperature of the bottom baffle considering conduction from the annulus to the bottom baffle directly, radiation through all the baffles, and conduction through the stack of baffles and washers. The net radiation exchange followed the same logic as equation (5-8), while the conduction was calculated with a conduction resistance network based on Fourier's Law, shown in equations (5-10) and (5-11).

$$q = \frac{T_{annulus} - T_{bottom\ baffle}}{R_{total}} \tag{5-10}$$

$$R_{tot} = \sum R_{contact} + \sum \frac{L}{A * k} \tag{5-11}$$

From equation (5-11), L is the path length of conduction, while A is the cross-section of that path and k is the thermal conductivity. As shown in equation (5-11), the resistance to conduction depends both on the material resistance and the contact resistance. The contact resistance for this analysis is significant, as the washers between the baffles were spring washers, chosen to create minimal contact and maximum path length to the baffles. Additionally, through the path from the annulus to the bottom baffle, the baffle is supported by pins with little contact to the baffles. While difficult to determine analytically, the contact resistances were estimated to be on the order of 100 K/W based on a prior empirical study [38]. The comparison of the heat transfer from the annulus by the three described paths is shown in Figure 5-7, where a lower temperature of the innermost baffle would lead to a larger heat transfer from the annulus.

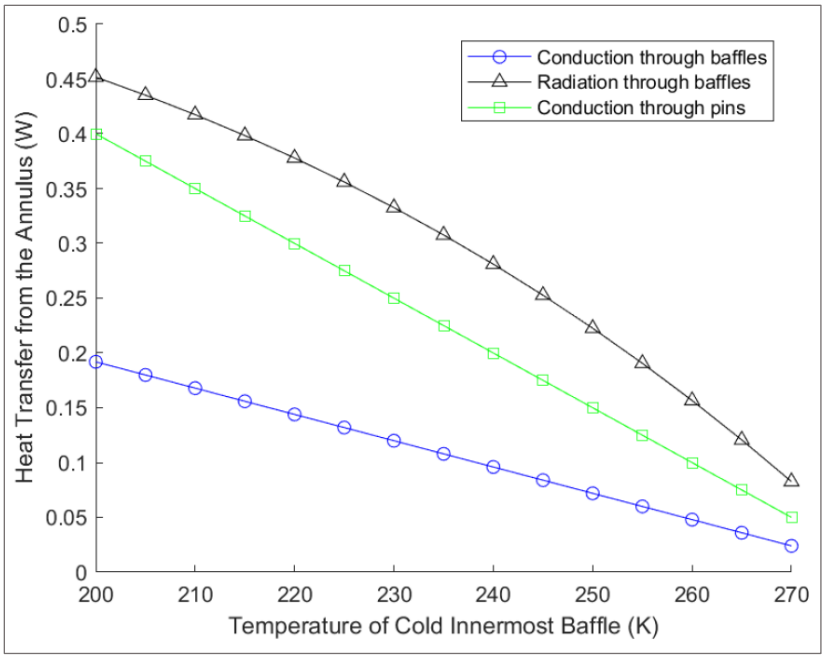

Figure 5-7: Heat transfer by path from the annulus at 280 K to the cold inner baffle

Following the analysis of the heat transfer from the annulus, it was important to integrate the results with the results from the shields of the MLI. As shown previously, the conductance of the Kevlar strings was sufficiently low to consider conduction negligible. Due to this fact, the interactions between the annulus and the vertical shields is strictly radiative. The radiation between the annulus and the shields was then calculated with a radiative resistance network from the bottom baffle to each of the fourteen shields. This network must inherently differ from the network used for the shields. Despite the complicated geometry, observations about the network reveals a shortcut to this analysis. A representative example of radiation from the baffle is shown beginning in Figure 5-8, which assumes that radiation leaving the baffle from any point on the baffle has a line of sight to two shields. This analysis also assumes an isothermal baffle. A description of the resistive elements is shown in Table 5.2, with individual resistance equations having been derived in equation (3-4).

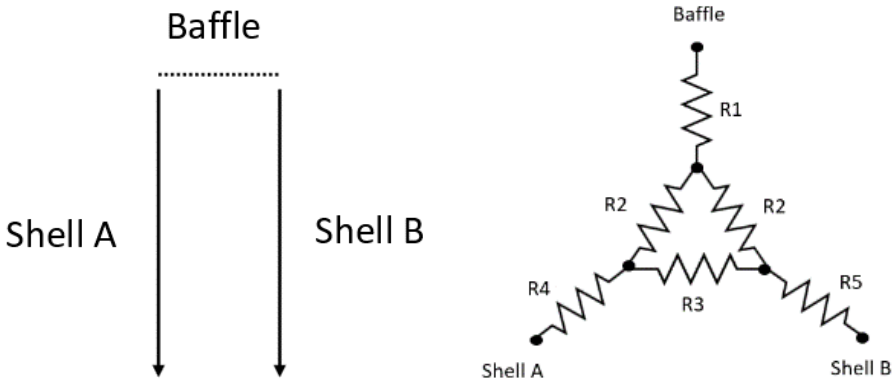

Figure 5-8: Three-body baffle-shield enclosure with semi-infinite shields

Table 5.2: Resistor descriptions for Figure 5-8

Resistor	Description
R1	Baffle emission
R2	Baffle to shield geometry
R3	Shield to shield geometry
R4	Shield A emission
R5	Shield B emission

By noting that the surface area of each shield is much larger than the baffles while the view factor, F, from one shield to the other is always above 0.9, resistor R3 is negligible compared to the other resistors in the system. This leads to the circuits shown Figure 5-9. This circuit can be further decomposed to conclude that the radiation from the baffle to each shield is a series circuit of resistors R1 to 0.5*R2 to R4. This leads to the final equation for the radiative interaction of the baffle and shields, equation

(5-12), for which the terms in the denominator containing ε are the resistance to emission, and the term containing the view factor is the geometric resistance:

$$Q = \sum_{i=1}^{14} \frac{\sigma(T_b^4 - T_i^4)}{\frac{1-\varepsilon_b}{\varepsilon_b A_b} + \frac{1}{2A_b F_{b-i}} + \frac{1-\varepsilon_i}{\varepsilon_i A_i}} \tag{5-12}$$

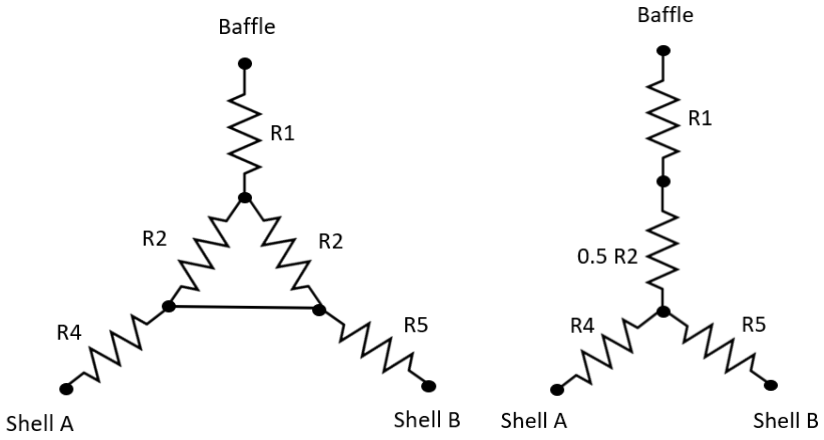

Figure 5-9: Simplified circuits assuming R3 is negligible

Once equation (5-12) was developed, it could be used to equate the sum of the heat transfer from the annulus to the baffle to the radiation from the baffle to the shields of the MLI. Specifically, equation (5-12) calculated for a range of baffle temperatures and compared with the sum of the heat transfer paths from the annulus to the baffle, which were shown in Figure 5-7. Figure 5-10 was plotted to solve for the equilibrium of heat into the baffle from the annulus and heat from the baffle to the MLI. The crossing point of the two curves shows that 0.34 W are transferred from the annulus to

the vertical shields of the MLI assembly, with the temperature of the bottom baffle at 256 K.

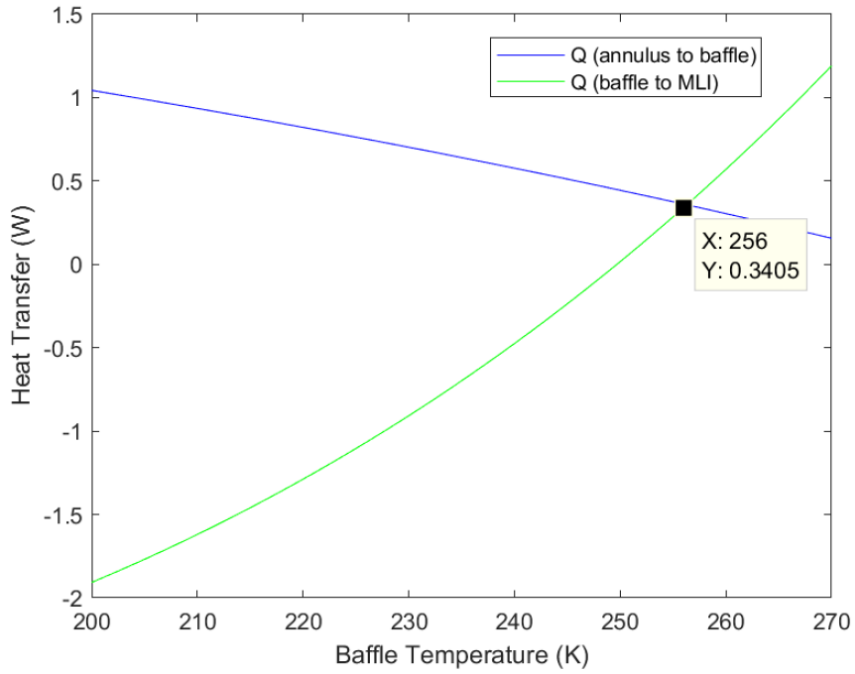

Figure 5-10: Comparison of the heat transfer from the annulus to the baffle and from the baffle to the MLI to determine the equilibrium temperature and heat transfer of the baffle (shown)

This analysis showed an important aspect of heat transfer within the MLI. The baffle temperature of 256 K was between the temperature of the ninth and tenth shields from the bucket, as determined in Figure 5-5. Shields 10-14 will be able to radiate to the baffle, which can offer a thermal shortcut to the inner shields by conducting the heat towards the cryogenic bucket and radiating to the inner shields. By looking at each term in equation (5-12), up to 0.39 W could be transferred from the shields to the baffle to shortcut the MLI. In total, heat transfer due to the annulus assembly could contribute 0.73 W. This is significant compared to the 1.04 W of heat transfer expected through the shields alone. Due to the geometry of the MLI, the component of the insulation that interacts with the bucket of the Dewar is the innermost radiation shield. Whereas the

innermost radiation shield would need to be 146 K to radiate 1.04 W to the bucket, to radiate 1.77 W, the temperature would rise to 164 K, considering a simple, two-body radiation exchange. The temperature rise of the innermost shield will also result in higher temperatures for the remaining shields, deviating from the profile established in Figure 5-5 to create a steeper curve. The inclusion of temperature sensors in the MLI will be vital to determining the exact heat transfer, as well as the relationship between the vertical shields and the annulus.

Section 5.2.3: Comparing BOBCAT-1 and BOBCAT-2 Thermal Analyses

At this point, three analyses have been conducted of the heat transfer in the BOBCAT payloads. Section 3.4 presented the estimates of the heat gain through the BOBCAT-1 conventional MLI system. Previous sections of this chapter have developed models for the heat transfer within the novel MLI of the BOBCAT-2 ultra-light Dewar. Section 5.2.1 presented an analysis of the ultra-light Dewar that strictly looked at heat transfer through the aluminized mylar shields that compose the bulk of MLI. Section 5.2.2 then integrated these results with an analysis of heat gain originating at the annulus of the Dewar and being transported through the thermal closeout assembly. This section will compare the results of these three analyses over the range of potential outer wall temperatures.

Prior discussion has treated the boundary condition of the outer wall of the ultra-light Dewar as a constant 280 K, a best estimate for the temperature of the wall at 40 km. With the range of atmospheric conditions above 24 km (217-261 K) and the potential for a 40 K temperature difference between the atmosphere and the payload, the temperature range considered was from 230-300 K. Table 5.3 presents a

comparison of the BOBCAT-1 analysis and the two BOBCAT-2 analyses over this range of conditions.

Table 5.3: Comparison of BOBCAT-2 thermal analyses to BOBCAT-1 estimates

Outer Wall Temperature (K)	BOBCAT-2 Shields (W)	BOBCAT-2 Shields and Annulus (W)	BOBCAT-1 (W)
230	0.47	0.83	0.076
240	0.56	0.98	0.090
250	0.66	1.15	0.11
260	0.77	1.34	0.12
270	0.90	1.55	0.14
280	1.04	1.77	0.16
290	1.20	2.03	0.19
300	1.37	2.33	0.22

Table 5.3 shows that the ultra-light Dewar MLI is expected to perform an order of magnitude less effectively than the conventional Dewar over a range of flight conditions. There are several reasons for this difference in performance. First and foremost, the ultra-light Dewar MLI system consists of only fourteen radiation shields, much less than can be achieved in tightly packed blankets of reflectors and spacers used in conventional MLI. The ultra-light Dewar used fourteen radiation shields to balance thermal performance against the large spacing between the shields to allow air flow out of the vessel on ascent. Additionally, due to the large spacing, BOBCAT-2 ultra-light Dewar had a 0.76-meter diameter outer wall compared to 0.36-meter diameter outer wall for the BOBCAT-1 conventional Dewar. For the 280 K outer wall case, the estimated 0.18 W through the walls of the conventional Dewar is equal to a flux of 0.12 Wm^{-2}, while for the ultra-light Dewar, the 1.77 W of total heat transfer is equal to a flux of 0.45 Wm^{-2}. The number of shields flown and the additional heat transfer from

the thermal closeout assembly are then believed to contribute the bulk of the difference in heat flux.

All told, for the 280 K outer wall case, the 1.77 W of heat transfer through the ultra-light Dewar MLI could contribute an additional 60% to the total heat that reaches the superfluid helium in the bucket, when considering the open aperture heat load experienced during BOBCAT-1. This would result in a total heat transfer of 4.4 W if the flight conditions were similar between BOBCAT-1 and BOBCAT-2. Considering that 2.6 W are likely due to the open aperture and that the BOBCAT project acts as a technology demonstration mission, achieving this result from the flight mission would show that the ultra-light Dewar concept functions as an adequate bucket Dewar.

Section 5.3: Instrumentation

Validating the fluid and thermal models of the ultra-light Dewar will be an important aspect of the BOBCAT project moving forward. After the flight experiment, the models will be critical for demonstrating an understanding of the underlying physics of the thermal environment within the ultra-light Dewar. The models could also show potential areas of deficient understanding, should the experiment not match these analyses.

The instrumentation for the ultra-light Dewar focuses on both the bucket and the vacuum space. For the bucket of the Dewar, the insert was kept largely the same as flown on BOBCAT-1, shown previously in Figure 3-2. The level sensors were kept the same for comparing the boiloff in the conventional and ultra-light Dewars. Due to channel limitations on the electronics boxes, the number of temperature sensors on the insert was required to remain the same. However, the opportunity existed to make

changes that would allow for deeper understanding of the heat transfer paths that were discussed previously. Improved understanding of the temperature profile of the helium gas during the boiloff process would also aid in determination of the convection from the walls of the bucket to the boiloff gas. This profile can be achieved by moving the redundant temperature sensor at the bottom of the bucket to halfway between the sensor near the middle of the insert and the sensor under the lid of the bucket. The sensor under the lid can then be moved to be under the exhaust at a similar height in the bucket to be fully in the flow of the boiloff gas out of the bucket. With these two, simple changes, shown in Figure 5-11, the new sensor scheme would capture the temperature of the superfluid helium as well at three points in the flow of gaseous helium out of the bucket, as opposed to the one sensor in the flow from BOBCAT-1.

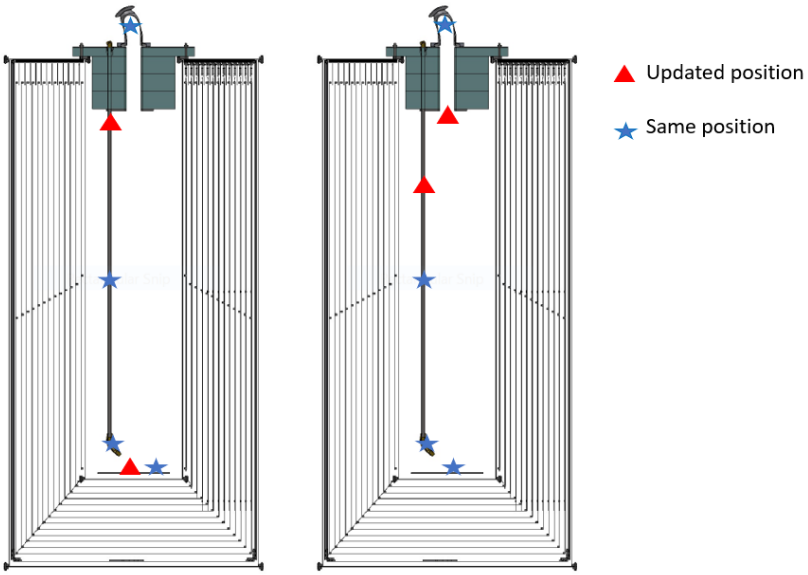

Figure 5-11: Left) Dewar insert diode scheme BOBCAT-1, right) updated diode scheme, BOBCAT-2

For the vacuum space of BOBCAT-2, additional instrumentation includes pressure and temperature sensors to monitor and record data for the novel MLI system. The pressure sensors are affixed to the five-way port connected to a vent line elbow, as

could be seen in Figure 4-18. The selected pressure sensors were an ion gauge and a Pirani gauge; the ion gauge will cover from 10^{-7}-10^{0} Pa, while the Pirani gauge covers from 10^{-2}-10^{5} Pa. The manufacturer reports a 15% uncertainty in the measurements at the low range of the sensors that drops as the pressure rises. The use of these two gauges will offer the full range of coverage from ambient pressure at sea level down to a vacuum. These pressure sensors will be used to explore the pressure within the vacuum space as the vessel ascends and confirm the model of the vent-on-ascent concept. The pressure sensors will also be used to ensure a vacuum is achieved when the bucket is filled with cryogen and that this vacuum is maintained over the course of the flight experiments. Any leak of air into the vacuum shell would serve as another heat transfer mode through the insulation, greatly increasing the heat transfer to the superfluid helium. Figure 5-12 shows the effects of heat transfer through an insulation system based on the pressure of air in the vacuum [39]. It shows that an MLI system will perform best with an interstitial pressure below 10^{-4} Torr (0.01 Pa), four orders of magnitude less than the ambient air at 40 km.

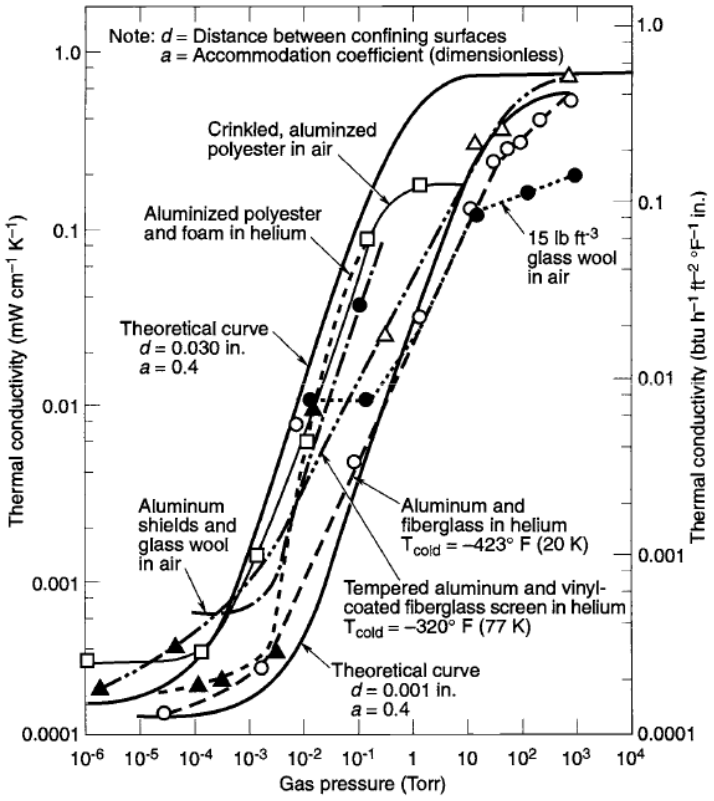

Figure 5-12: Effect of interstitial pressure on MLI effectiveness [39]

In addition to the pressure sensors, the ultra-light Dewar will include thermal diodes (DT-670s from Lakeshore Cryogenics) to determine the temperature gradient and heat transfer through the MLI system. The vendor reports an uncertainty of 22 mK at 77 K and 32 mK at 300 K. With the current limits to the electronics boxes, eight diodes were chosen. The scheme for arranging these eight diodes is shown in Figure 5-13.

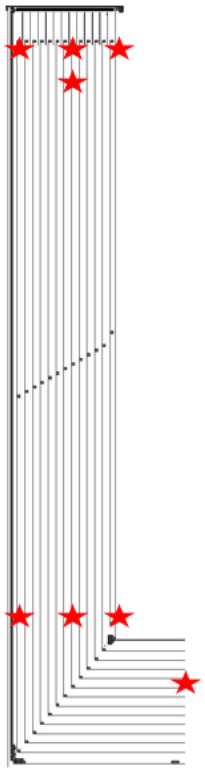

Figure 5-13: Diode placement within the MLI of the ultra-light Dewar

The choices for alignment were made so that placing diodes on three shields would establish the temperature gradient through the MLI system. This gradient is created by keeping the eight diodes in a single angular plane of the cylindrical vessel. The innermost shield diodes will allow for a good estimate of the total heat transfer to the bucket, as the radiation from the innermost shield is expected to be the dominant heat path through insulation. Using the specifications reported by the vendor and equation (5-13), the uncertainty in the heat transfer from the innermost shield to the cryogenic bucket would be 10^{-3} W for a shield temperature of 150 K. This uncertainty would climb to 0.02 W for the diodes on the outermost shield with a shield temperature of 280 K. In equation (5-13), dq/dT is the derivative in the heat transfer in terms of

temperature and U refers to the uncertainty. The heat transfer for the two-body system can be obtained from a simpler version of equation (3-3), as mentioned previously.

$$U(q) = \sqrt{(\frac{dq}{dT})^2 * u(T)^2} \tag{5-13}$$

The diodes on the 6th and 13th layers help to establish the temperature gradient. The three shields have diodes placed at the top of the shield, near the exchange with the annulus to explore the ratio of the heat transfer through the annulus and through the shields. On the 6th shield, an approximate middle shield, there will be four total diodes. The diode offset from the top by 10 cm will be used to verify the assumption of isothermal shields and determine how deep the heat transfer from the annulus penetrates. The diode on the drumhead of this shield will be used to confirm that the temperature and heat flux from the drumheads will be comparable to the sides. By including these diodes, and the other instruments discussed, the flight experiment for BOBCAT-2 will create a robust dataset to lead to a fuller understanding of the thermal and fluid environments in the novel ultra-light Dewar.

Section 5.4: Scalability

The previous sections of Chapter 5 presented models of the ultra-light Dewar for the BOBCAT-2 flight missions; this section will take a brief look at the scalability of this design for 3-meter optical components. As was discussed in Chapter 2, prior balloon-borne payloads such as PIPER and ARCADE-2 deployed 1-meter scale optics aboard conventional bucket Dewars weighing 800 kg without cryogens or optical components. The PIPER payload has storage capacity for 3500 L and has a 1.5-meter bucket to store the 1-meter optics. The maximum deployable weight aboard high-

altitude balloons is roughly 2800 kg. The calculations in this section will neglect the weight of the optical components, electronics, and additional storage Dewars and instead discuss achieving comparable weight of the scaled ultra-light Dewar to the Dewars from PIPER and ARCADE-2.

The calculations performed here linearly scale the diameter and depth of the cryogenic bucket of the Dewar while keeping constant wall thickness and radial space for the novel MLI system. Using the bucket dimensions of PIPER with the ultra-light Dewar wall thickness and radial space for the novel MLI system, the ultra-light Dewar would weigh under 150 kg when scaled to the size of PIPER. Further scaled to house 3-meter optics, the ultra-light Dewar would weigh 1100 kg with a wall thickness of 0.6 mm and a storage volume of 100,000 L. At this size, the ultra-light Dewar weighs nearly 40% more than the PIPER dewar, without accounting for cryogen. This can be reduced if the storage volume of the Dewar is not needed to scale with the diameter, where at a Dewar diameter of 4.5-meters housing 3-meter optics, decreasing the depth of the Dewar by 33% yields a Dewar mass of 800 kg. Additionally, section 5.1.1 established that the 0.6 mm wall thickness, chosen to match vendor capabilities, is oversized. Even for 0.1 mm wall thickness at 30 km in altitude, the hoop stress on the wall is a fourth of the yield stress of the material, using equation (5-1). With 0.1 mm thick walls, the ultra-light Dewar scaled to house 3-meter optics would weigh less than 200 kg. These calculations establish that scaled versions of the BOBCAT ultra-light Dewar will be capable of achieving significant weight savings over conventional bucket Dewar technology.

Chapter 6 Conclusions and Future Work

Through the first five chapters of this thesis, the BOBCAT project was presented. The goal of the BOBCAT project is to greatly reduce the weight of cryogenic bucket Dewars aboard high-altitude balloon payloads in order to increase the allowable telescope size. This thesis detailed the flight and post-flight data analysis of the BOBCAT1 payload, which flew a conventional bucket Dewar. The conventional bucket Dewar was flown both to demonstrate cryogen transfer at a float altitude and to establish baseline thermal performance for comparison to the ultra-light Dewar from BOBCAT2. For the BOBCAT2 ultra-light Dewar, this thesis detailed prototyping, design improvements, and assembly that took the ultra-light Dewar from initial designs to a flight-ready vessel. Detailed analyses were also conducted to establish expected performance of the Dewar as it vents on ascent and heat transfer through the MLI while the flight experiments are performed. Successfully meeting these goals would constitute a major step forward in the development of the ultra-light Dewar concept for larger aperture, cryogenic, balloon-borne payloads.

Section 6.1: Conclusions

The contributions of this thesis to the BOBCAT project are summarized as follows:

1. The launch operations and flight experiment of the BOBCAT-1 payload were performed

2. Post-flight data analysis verified the success of cryogen transfer aboard BOBCAT-1 and established the baseline heat gain of the conventional bucker Dewar
3. Two prototypes were constructed to verify and improve design and assembly of the ultra-light Dewar concept
4. Radiation shields of the novel MLI system for the BOBCAT-2 ultra-light Dewar were successfully assembled and integrated with the vacuum shell
5. Fluid models of the vent-on-ascent and cryoplating concepts were developed
6. Thermal models of the ultra-light Dewar MLI were derived and compared to the BOBCAT-1 results

Section 6.2: BOBCAT-2 Future Work

The designs, expected performance for flight, and flight logic of the BOBCAT-2 mission have been discussed in the prior sections of this thesis, and this final section will formally present the complete flight plan for the BOBCAT-2 payload. As with each prior NASA balloon payload, launch operations will be performed by CSBF, utilizing either the early or late summer launch sites of Palestine, Texas, or Fort Sumner, New Mexico. The prelaunch and launch procedures will be largely the same as those presented in Chapter 3 for the BOBCAT-1 launch.

The launch campaign of the BOBCAT-2 mission will differ from BOBCAT-1 in a couple important ways. The first way is that the ultra-light Dewar must be checked for hermeticity on arrival to the launch site. As Chapter 4 showed, there is some concern regarding the fragility of the vacuum vessel, especially considering transportation. Loss

of hermeticity of the vessel would prevent the ultra-light Dewar from functioning as an efficient cryogen storage device by introducing convection as a heat transfer mode through the MLI. For the second change to the pre-flight work, the ultra-light Dewar cannot undergo a cryogen test prior to launch. Transferring cryogen to the bucket on the ground would create a vacuum and a pressure difference large enough to catastrophically damage the Dewar.

On launch day, the procedures will be similar to the BOBCAT-1 flight. On ascent, in addition to monitoring the temperature of electronic and motor components, the pressure in the insulation space will be watched closely from the readouts of the pressure sensors. Atmospheric pressure versus the pressure in the insulation space will be frequently compared, as well as recorded, to determine the fidelity of the vent-on-ascent model. At float altitude, the butterfly valve will be used to seal the insulation space, and cryogen transfer will proceed similarly to BOBCAT-1. Following the cryogen transfer, the pressure in the vacuum space will be closely monitored to confirm that a vacuum is achieved and held by the cryoplating method. This pressure will be checked often during the experiment to ensure the integrity of the vacuum created. After the cryogen fill, the boiloff experiment will proceed in the same way as BOBCAT-1. Following the experiment, the butterfly valve will be opened to aid in boiling off the remaining cryogen from the storage vessels to aid in safe landing and recovery. The ultra-light Dewar was not designed to survive any condition beyond a smooth landing, so recovery of an undamaged ultra-light Dewar is not a criterion for success.

After the flight and recovery of the BOBCAT-2 payload, significant work will remain to quantify the success or failure of the mission, specifically in the context of the feasibility of the ultra-light Dewar concept. The first post-flight analysis will be the calculation of the boiloff rate of the superfluid helium to determine the heat transfer calorimetrically. This will proceed in the same manner as was done for BOBCAT-1. Then, comparing the temperature values calculated by the thermal model to the true value returned by the diodes will be critical to understanding the thermal environment within the ultra-light Dewar. Afterwards, the first two phases of the BOBCAT mission will be complete and will demonstrate the feasibility of using an ultra-light bucket Dewar to achieve 3-4-meter observatories at high altitude.

Appendix A: Ultra-Light Dewar MLI Temperature Profile with Varying Boundary Conditions

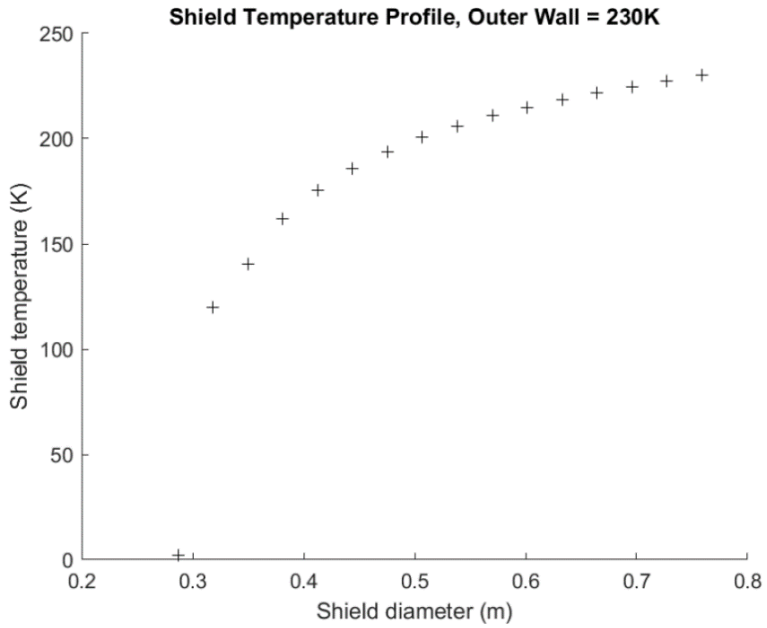

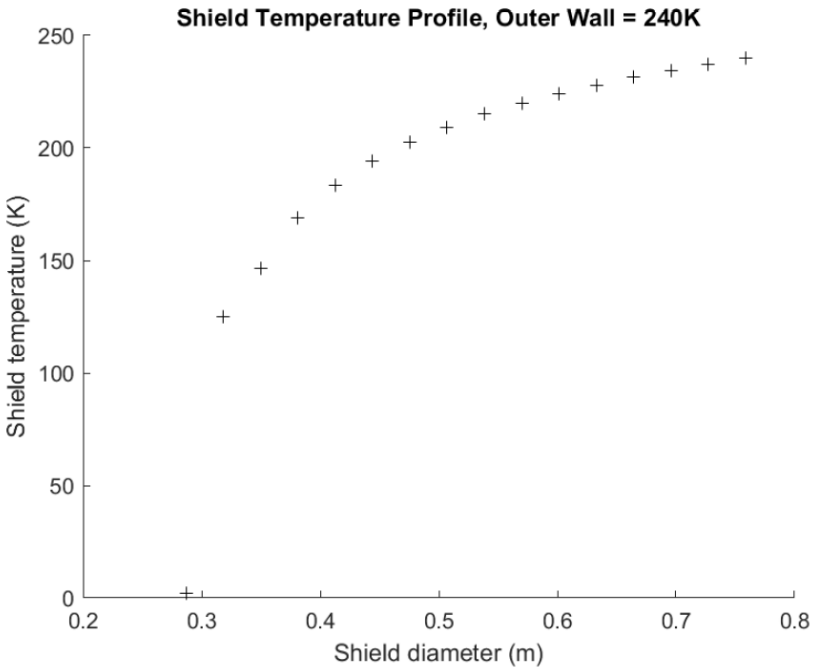

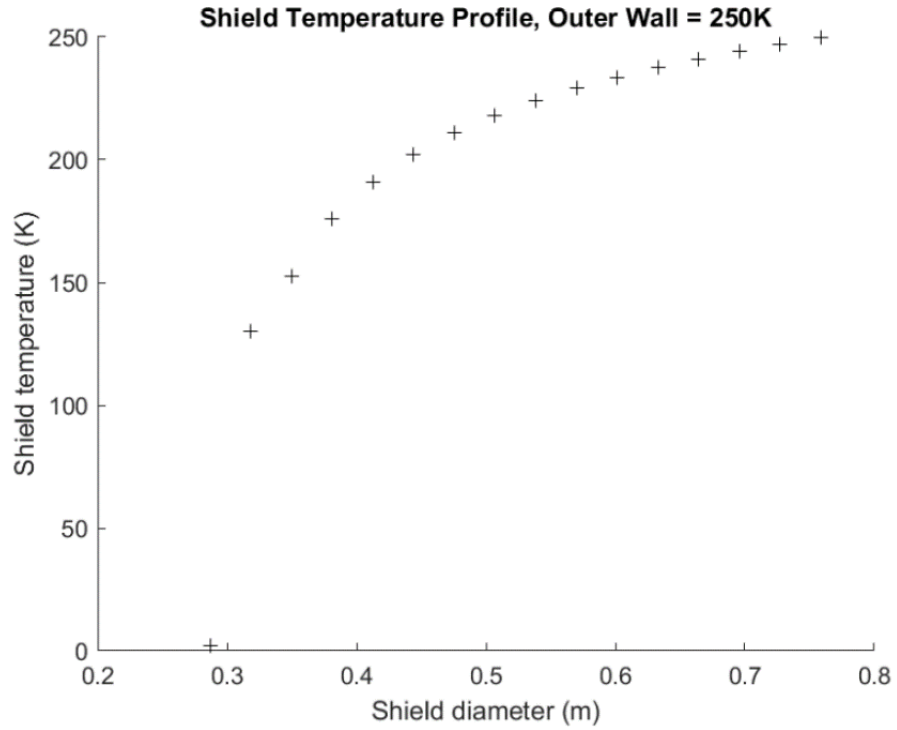
Shield Temperature Profile, Outer Wall = 250K
Shield temperature (K)
Shield diameter (m)
0
50
100
150
200
250
0.2
0.3
0.4
0.5
0.6
0.7
0.8

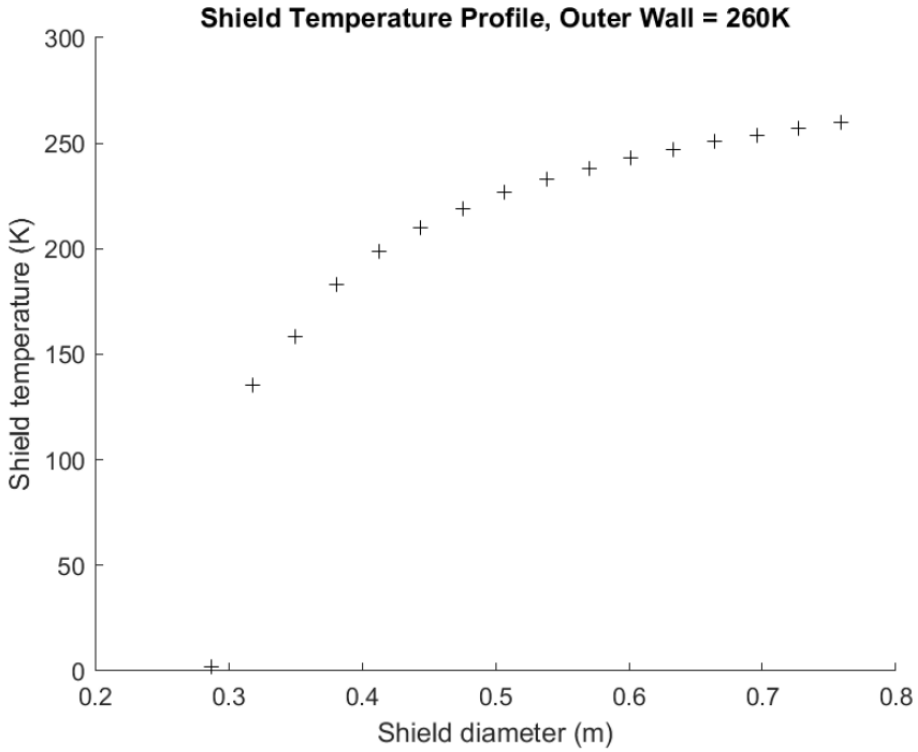
Shield Temperature Profile, Outer Wall = 260K
Shield temperature (K)
Shield diameter (m)
0
50
100
150
200
250
300
0.2
0.3
0.4
0.5
0.6
0.7
0.8

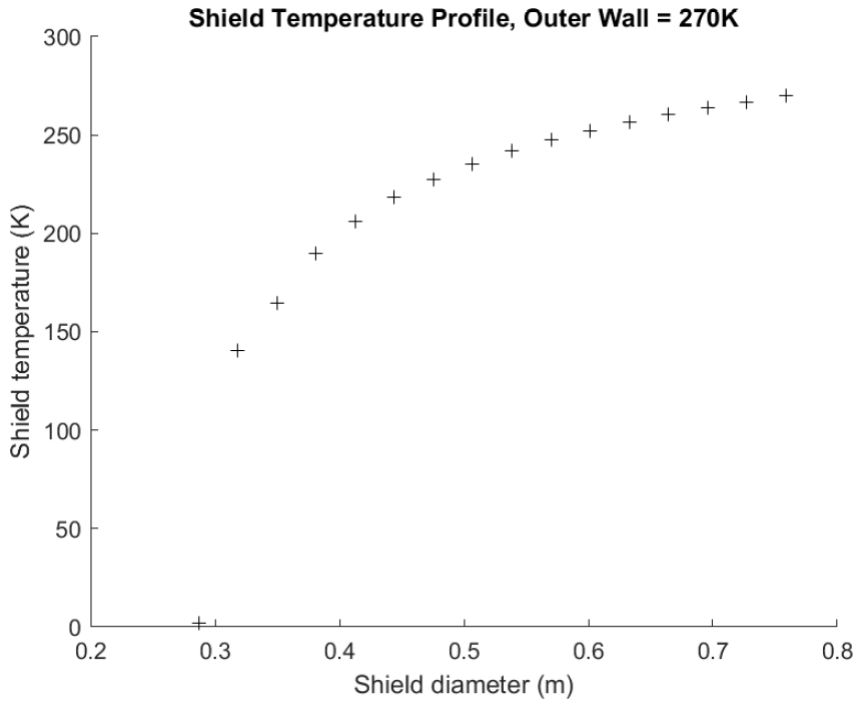
Shield Temperature Profile, Outer Wall = 270K
Shield temperature (K)
Shield diameter (m)
0
50
100
150
200
250
300
0.2
0.3
0.4
0.5
0.6
0.7
0.8

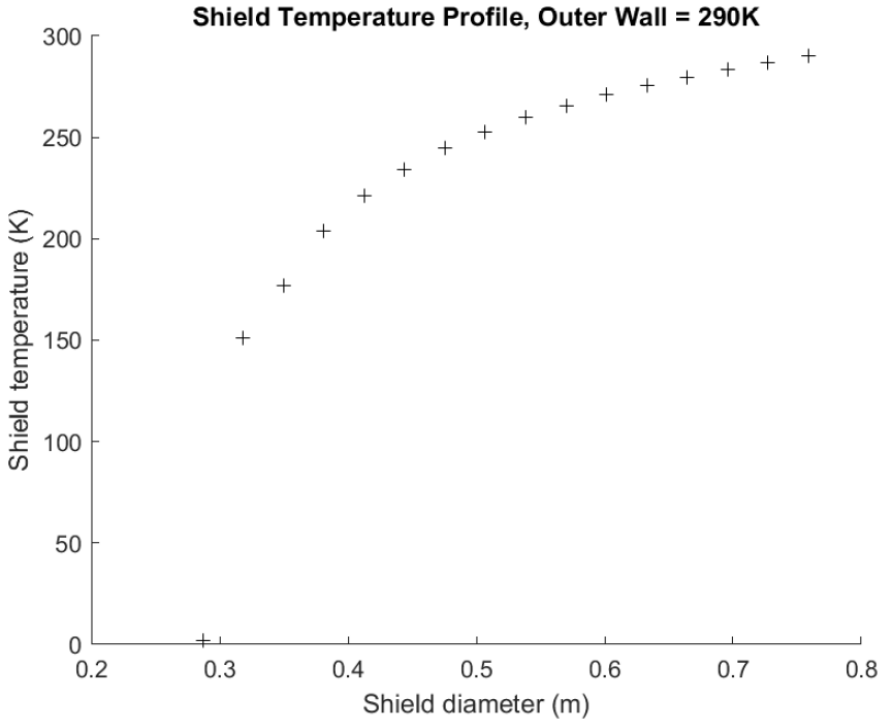
Shield Temperature Profile, Outer Wall = 290K
Shield temperature (K)
Shield diameter (m)
0
50
100
150
200
250
300
0.2
0.3
0.4
0.5
0.6
0.7
0.8

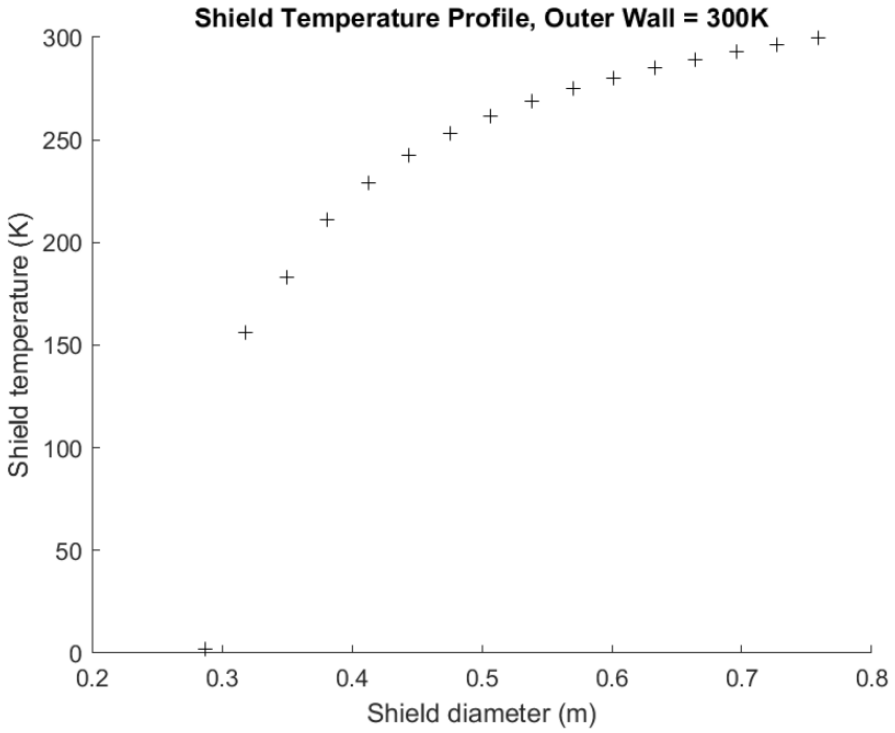
Shield Temperature Profile, Outer Wall = 300K
Shield temperature (K)
Shield diameter (m)
0
50
100
150
200
250
300
0.2
0.3
0.4
0.5
0.6
0.7
0.8

Bibliography

[1] A. Kogut, S. Denker, N. Bellis, et al. "Bulk Cryogen Transfer at 40 km Altitude" Submitted to: *Cryogenics,* 2020

[2] G. J. Stacey, S. Hailey-Dunsheath, C. Ferkinhoff, et al. "A 158 Mm [C Ii] Line Survey of Galaxies at Z∼1-2: An Indicator of Star Formation in the Early Universe." *The Astrophysical Journal*, vol. 724, no. 2, Oct. 2010, pp. 957–974.,

[3] D. Leisawitz. "NASA's Far-IR/Submillimeter Roadmap Missions: SAFIR and SPECS." *Advances in Space Research*, vol. 34, no. 3, 2004, pp. 631–636.

[4] D. Leisawitz, E. Amatucci, R. Carter, et al. "The Origins Space Telescope: Mission concept overview." *Proceedings of SPIE* vol. 10698, 2018.

[5] C. Qi. "The Submillimeter Array." *Advances in Space Research*, vol. 40, no. 5, 2007, pp. 639–643.

[6] E. F. Erickson, J. A. Davidson. "SOFIA: Stratospheric Observatory for Infrared Astronomy." *Advances in Space Research*. vol. 13, no. 12, 1993, pp. 549–556.

[7] M. J. Griffin, et al. "The Herschel-SPIRE Instrument and Its In-Flight Performance." *Astronomy and Astrophysics* vol. 518, 2010

[8] J. Lazear, et al. "The Primordial Inflation Polarization Explorer (PIPER)" *Proceedings of SPIE,* vol. 9153, 2014

[9] Kogut, A., et al. "ARCADE: Absolute Radiometer for Cosmology, Astrophysics, and Diffuse Emission." *New Astronomy Reviews*, vol. 50, 2006, pp. 925–931

[10] E. Pascale, et al. "The Balloon-Borne Large Aperture Submillimeter Telescope: BLAST." *The Astrophysical Journal,* vol. 681, no. 1, 2008, pp. 400–414.

[11] E. Urban. "Emergency Relief Venting of the Infrared Telescope Liquid Helium Dewar" Technical Report: *NASA-TM-82420*, NASA, 1981.

[12] T. N. Fleener. "A Low-Cost Space-Qualified Superfluid Helium Dewar." *Cryogenics*, vol. 39, no. 8, 1999, pp. 697–699.

[13] V. L. Pereguda, and D. L. Storozhik. "Manufacture of Welded Thin-Walled Cryogenic Dewar Vessels from AMtsS Alloy." *Chemical and Petroleum Engineering*, vol. 15, no. 12, 1979, pp. 938–941.

[14] J. E. Fesmire, and W. L. Johnson. "Cylindrical Cryogenic Calorimeter Testing of Six Types of Multilayer Insulation Systems." *Cryogenics*, vol. 89, 2018, pp. 58–75.

[15] S. D. Augustynowicz, and J. E. Fesmire. "Cryogenic Insulation System for Soft Vacuum." *Advances in Cryogenic Engineering,* 2000, pp. 1691–1698.

[16] M. E. Riesco, et al. "Venting and High Vacuum Performance of Low-Density Multilayer Insulation." *AIP Conference Proceedings,* 2010

[17] W. L. Johnson. "Thermal Performance of Cryogenic Multilayer Insulation at Various Layer Spacings." Master of Science Thesis. University of Central Florida, Orlando, 2010.

[18] J. B. Heaney. “Efficiency of Aluminized Mylar Insulation at Cryogenic Temperatures.” *Cryogenic Optical Systems and Instruments VIII*, 1998.

[19] W. L. Johnson, N. T. Van Dresar, D. J. Chato, J. R. Demers “Transmissivity Testing of Multilayer Insulation at Cryogenic Temperatures.” *Cryogenics*, vol. 86, 2017, pp. 70–79.

[20] F. Rodger. “BalloonAscent: 3-D Simulation Tool for the Ascent and Float of High-Altitude Balloons.” *AIAA 5th ATIO and 16th Lighter-Than-Air System Technology and Balloon Systems Conferences*, 2005

[21] F. Kreith and J. C. Warren. “Thermal Analysis of Balloon-Borne Instrument Packages” Technical Report: *NCAR-TN-45*, University Corporation for Atmospheric Research, 1970.

[22] R. J. Donnelly and C. F. Barenghi. “The Observed Properties of Liquid Helium at the Saturated Vapor Pressure.” *Journal of Physical and Chemical Reference Data*, vol. 27, no. 6, 1998, pp. 1217–1274.

[23] N. N. Filina. “The Boiling of Superfluid Helium” *Chemical and Petroleum Engineering*, vol. 37, nos. 7–8, 2001

[24] W. F. Giauque, and J. O. Clayton. “The Heat Capacity and Entropy of Nitrogen. Heat of Vaporization. Vapor Pressures of Solid and Liquid. The Reaction 1/2 N2 1/2 O2= NO from Spectroscopic Data.” *Journal of the American Chemical Society*, vol. 55, no. 12, 1933, pp. 4875–4889.

[25] “Earth Atmosphere Model - Metric Units.” *NASA*, NASA, URL: www.grc.nasa.gov/WWW/K-12/airplane/atmosmet.html.

[26] C. W. Keller, G. R. Cunnington, A. P. Glassford. “Thermal Performance of Multi-Layer Insulations” Technical Report: *NASA-CR-134477,* NASA, Lockheed Missiles and Space Company, 1974.

[27] A. W. Knudsen. “Metallic Vacuum-Tight Gasket.” *Review of Scientific Instruments*, vol. 23, no. 10, 1952, pp. 566–567.

[28] “304 Stainless Steel.” *MatWeb* URL: matweb.com/search/DataSheet.aspx?MatGUID=abc4415b0f8b490387e3c922237098da.

[29] G. P. Brasseur, and S. Solomon. *Aeronomy of the Middle Atmosphere: Chemistry and Physics of the Stratosphere and Mesosphere*. Springer, 2005.

[30] T. R. Strobridge. “The Thermodynamic Properties of Nitrogen from 64 to 300℃K between 0.1 and 200 Atmospheres.” *U.S. Dept. of Commerce, National Bureau of Standards*, 1962.

[31] H. Shakeel, H. Wei, and JM Pomeroy. “Measurements of Enthalpy of Sublimation of Ne, N2, O2, Ar, CO2, Kr, Xe, and H2O Using a Double Paddle Oscillator.” *The Journal of Chemical Thermodynamics*, vol. 118, 2018, pp. 127–138.

[32] G. Ventura and V. Martelli. “Thermal Conductivity of Kevlar 49 between 7 and 290K.” *Cryogenics*, vol. 49, no. 12, 2009, pp. 735–737.

[33] M. M. Finckenor and D. Dooling. “Multilayer Insulation Material Guidelines” Technical Report: *NASA/TP-1999-209263,* NASA, 1999.

[34] L. Vegard. “Crystal Structure of Solid Nitrogen.” Nature, vol. 124, no. 3122, 1929, pp. 337–337.

[35] E. D. Marquardt, et al. “Cryogenic Material Properties Database.” *11th International Cryocoolers Conference*, 2002, pp. 681–687

[36] D. B. Mann. “Liquefied Natural Gas Research at the National Bureau of Standards” *Publication Number: 80-1636,* 1980

[37] J. H. Henninger. “Solar Absorptance and Thermal Emittance of Some Common Spacecraft Thermal Control Coatings.” Technical Report: *NASA-RP-1121,* NASA, 1984.

[38] L. S. Fletcher and D. A. Gyorog. “Thermal Conduction Contribution to Heat Transfer at Contacts: An Analytical and Experimental Study of Thermal Contact Resistance of Metallic Interfaces” Technical Report: *NASA-CR-114373,* NASA, Arizona State University, 1968.

[39] D. G. Gilmore, M. Donabedian. *Spacecraft Thermal Control Handbook*. American Institute of Aeronautics and Astronautics, 2003.